FIRST PRINCIPLE DFT CALCULATION OF $MAPbX_3$ (X=Cl, Br, I) PEROVSKITES

A DISSERTATION

Submitted in partial fulfilment of the requirements for the award of the degree

of

MASTER OF TECHNOLOGY

in

NANOTECHNOLOGY

by

CHANDRA PRAKASH SAMARIYA

CENTRE OF NANOTECHNOLOGY

INDIAN INSTITUTE OF TECHNOLOGY ROORKEE

ROORKEE - 247667 (INDIA)

MAY, 2019

CANDIDATE'S DECLARATION

I hereby declare that the work presented in the dissertation entitled **"FIRST PRINCIPLE DFT STUDY OF $MAPbX_3$ (X=Cl, Br, I) PEROVSKITES"** submitted in partial fulfilment of the requirement for the award of degree of **Master of Technology** in **Nanotechnology, Indian Institute of Technology Roorkee,** is an authentic record of my own work carried out under the supervision of **Dr. Soumitra Satapathi,** Assistant Professor, Department of Physics, IIT Roorkee.

The matter presented in this dissertation has not been submitted by me for the award of any other degree of this or any other institution.

(Chandra Prakash Samariya)

Enrolment No. 17551002

Date:

CERTIFICATE

This is to certify that the above statement made by the candidate is correct to the best of my knowledge.

(Dr. Soumitra Satapathi)

Supervisor

Assistant Professor

Department of Physics

Indian Institute of Technology Roorkee

Abstract

Recent improvements in quantum mechanical theory algorithms has enabled more precise quantum mechanical calculations of advanced materials. Due to these algorithmic improvements more accurate theoretical modelling is now possible from which one can calculate and study material properties that were very challenging before. In last few years, Methyl Ammonium Lead Halide ($MAPbX_3$) has attracted more attention because of its high efficiency in solar cells. Here in this research work, first principle DFT calculation is performed to study optimized crystal structure, electronic and elastic properties of the Methyl Ammonium Lead Halide perovskites using two different exchange-correlation functional namely local density functional and generalised gradient exchange correlational functional. The properties calculated from this study is closely in agreement with the literature and experimental data. This study successfully calculated the optimized crystal structures, electronic structures, E-V plot for the $MAPbX_3$ (X=Cl, Br, I) perovskites.

In the very first chapter of this dissertation, very basic information about perovskite materials and first principle calculation is represented. The importance of first principle DFT over other methods is explained. In the next chapter, the literature review is done. It included the literature and articles related to the application and evolution of solar energy as a renewable energy alternative. Further, evolution of density functional theory (DFT) and its backbone in the form of theorems, are briefly introduced with the help of research papers. After that various first principle DFT study on Methyl Ammonium Lead Halide perovskites reported since few years, are represented with the help of research papers summary. The third chapter of this dissertation work gives detailed summary of the density functional theory background, its evolution, approximation used and some important equations and methods used during the DFT calculation. Thus it sets theoretical background for first principle DFT calculation. In the fourth chapter, computational details of first principle DFT like DFT package code used for the calculation, computational parameter calculations are described. The fifth chapter gives details about the synthesis of perovskite material film. It also tells about the characterization techniques used for the study of synthesized perovskite films. To calculate energy band gap value of perovskite films, UV-vis spectroscopy is done and Tauc plot is drawn for the band gap values. For the confirmation of successful perovskite film synthesis, XRD analysis is done which confirms the formation of the perovskite films without any other impurity. To analyse the topographic details of crystals formed and arrangement of overall crystals, FE-SEM image is taken. In sixth chapter of this study, plot of calculated electronic structures with density of states plot, optimized structures are attached. A comparative study between experimental and calculated parameters is done in this section. In the next chapter possible reasons (explanations) for the acquired results with concluding remarks are given. Final chapter makes the reference section of this dissertation.

ACKNOWLEDGEMENT

I am grateful to my mentor, **Dr. Soumitra Satapathi,** whose expertise, understanding and generous guidance made it possible for me to work on a topic that was of great interest to me. Without his valued suggestion and assistance, this research work would not have taken its present shape. It has indeed been an enriching scientific experience and I would like to thank him for providing me an opportunity to work under his guidance.

I owe my special thanks to Head of Centre of Nanotechnology, **Dr. R. K. Dutta** for providing me the best resources for my work. I am highly indebted to my seniors Mr. Amar Kumar and Mr. Naveen Kumar Tailor during the period of this work. I would extend my thanks to technical and non-technical staff of Centre of Nanotechnology and IIC (Institute Computer Centre) for their invaluable help and support.

Chandra Prakash Samariya

CONTENTS

LIST OF FIGURES

LIST OF TABLES

CHAPTER – 1

INTRODUCTION

1. General Introduction

The quantum mechanical theory has guided us to a development in understanding fundamental physics of materials. Quantum physics revealed surprisingly accuracy and great predicting capabilities. In order to model the complex materials and calculate relevant properties then the quantum mechanics equation has to be solved. But the fundamental equation of quantum mechanics i.e. Schrodinger's equation cannot be solved analytically for complex systems. So to make some meaningful development the equations of quantum mechanics must be solved computationally.

1.1 Electronic Structure Calculation:

For problems which cannot be solved analytically, computers with the help of numerical methods and simulations comes in handy. Firstly calculation of the analytically complex many body Schrodinger equation was done by Hartree and Fock, who made a set of self-consistent wave function equations which resulted in energy and other parameter calculation. This method introduced by Hartree and Fock had some limitations. The high cost of computation for the large systems was one of them. This arises from the many body wave function dependence on 3N spatial variables for N electron system, thus with increase in the size of system the variables and computational cost also increased.

1.2 Density Functional Theory:

To solve this problem and lower the cost of computation, Hohenberg and Kohn introduced a new approach in 1964. [1] They proved that the electron density, a single variable depending on 3 degree of freedom, alone contains the information needed about ground state of a system and its properties. This new approach is called "Density Functional Theory". In DFT Walter Kohn and L. J. Sham derived self-consistent equations which basically uses the concept of Hohenberg and Kohn in actual computer simulations. As the electron density is less complex entity than wave function, the cost of computation of DFT are very small than pure quantum mechanical approach of Hohenberg and Kohn.

1.3 First Principle Calculation:

The first principle method is basically ab-initio method which means it takes the basic information as input (crystal structure generally) and uses a series of simple

approximations (naïve approximations) without any fitting variable or entity. This type of calculation contains only the very basic description of the system without any requirement of extrinsic parameters. To be more precise, the interaction of the electrons is described using very general principles alone as an example the fundamental laws of quantum mechanics along with Schrodinger equation and the simulation are said to be ab initio calculation or first principle method. First principle calculation includes quantum mechanical calculation using Density Functional Theory without any requirement of higher order parameters. In practice, the density functional theory contains approximations for the electron-electron interaction thus limits the true accuracy.

1.4 Perovskite Materials:

Perovskites can be any material with structure similar to crystal structure of calcium titanium oxide ($CaTiO_3$). Originally perovskite was discovered in Russia and named after Russian mineralogist Lev Perovski. This material is also found in earth mantel. [2] The general formula for the perovskite compound in ABX_3 where X is anion, and A, B are cations. Usually B refers to the metal cation, having coordination number 6 i.e. cation B is surrounded with 6 X ions to make an octahedral geometry whereas the larger cation A fills the octahedral hole as shown in the Figure.

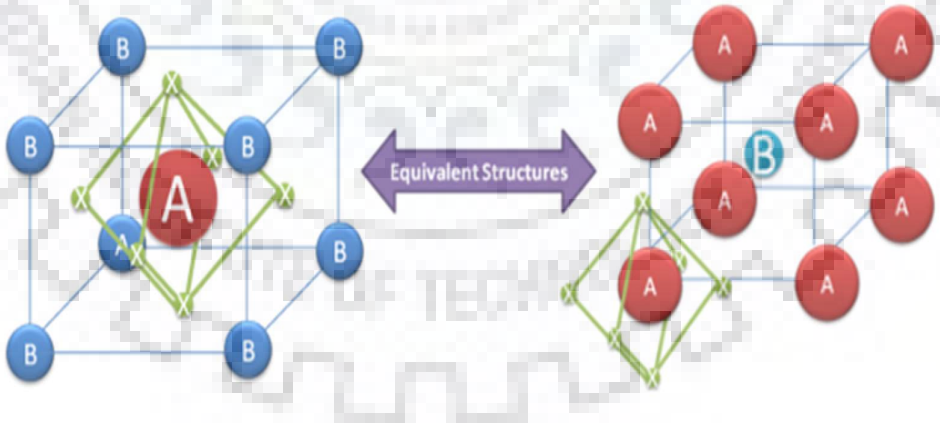

Fig. 1.1: Perovskite crystal structure. Taken with permission from Ref [2]

In these perovskites materials, A-site is a divalent metal A^{2+} cation (such as Mg^{2+}, Ca^{2+}, Sr^{2+}, Ba^{2+}, Pb^{2+}) in the centre of the lattice unit, the B-site is a B^{4+} cation (such as Ti^{4+},

Si^{4+}, Mn^{4+}, Fe^{4+}) around the A cations, and located in the centre of halogen oxygen anions. In addition, some carbides, nitrides, halides, and hydrides also crystallize in this structure. The flexibility to accommodate about all the element in periodic table and variety of properties exhibited makes it interesting. [2]

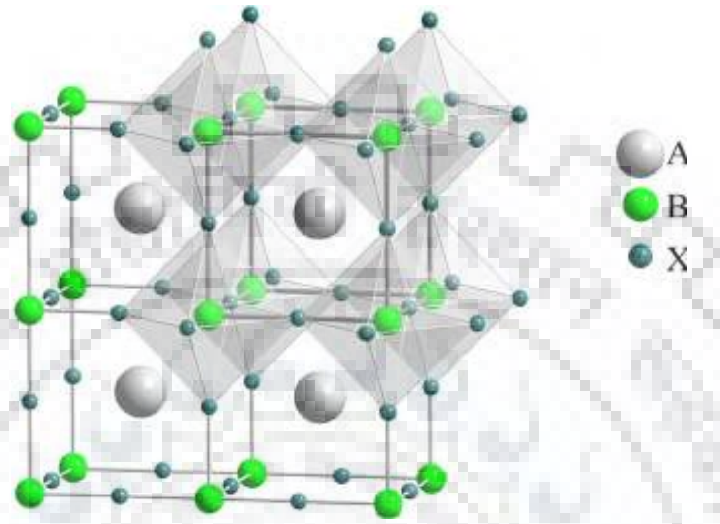

Fig. 1.2: ABX_3 ideal perovskite structure shows halogen (X) octahedron containing the B ion linked through corners to form a three dimensional cubic lattice taken with permission from Ref [2]

Despite the very simple original perovskite crystal structure, this family of compounds exhibits enormous number of structural modifications. Distorted perovskites have reduced symmetry which is a plus for their magnetic and electrical properties.

The perovskite structure type is given by tolerance factor [2] which is represented as,

$$t = \frac{R_A + R_X}{\sqrt{2}.(R_B + R_X)}$$

Where R_X, R_A, and R_B are the ionic radii of X, A and B onsite elements respectively. The tolerance factor (t) provides the suitability of different cation with different radius incorporated in octahedral holes. It helps in estimation of degree of distortion in the structure. If the A ion is smaller than ideal value then tolerance factor becomes less than 1 and $[BX_6]$ octahedron will tilt inwards to fill the space and lowering the symmetry. As perovskite is not true ionic compounds, the tolerance factor approach is an approximate estimate. Ideally its value varies from 0.75 to 1.

Another reason for structural modification is John-Teller effect. In some cases distortions can be aroused from some transition metal configuration at B position. Odd number of electrons in e_g and t_{2g} during d- orbital splitting leads to elongation of $[BX_6]$ octahedron.

Of the many ABX_3, though there are a lot of choices for perovskite materials but only those material can be use as light harvesting material which have high mobility (μ), optimum band gap, and energetic for efficient charge transport. Out of different perovskite structures and materials, organic-inorganic perovskites are particularly interesting due to tuneable band gap by tuning the halide and cationic element, high and equal mobility (μ) of excitons, large absorption coefficient and high efficiency. Other than that in perovskite, the separation of holes and electrons generated is comparatively easy as the diffusion length of excitons are over 1 μm which is long enough to avoid the excitons recombination process. Methyl Ammonium Lead Halide ($MAPbX_3$), X=I, Br, Cl, perovskites are one such type of perovskites having all of the above properties perfect for being implemented in solar cells.

CHAPTER – 2

LITERATURE REVIEW

2 Review of Literature

2.1 Perovskite based solar cells evolution

Today our society is facing rapid depletion of non-renewable energy resources. So one has to find out the renewable energy resources to supply the energy demand for the growing industries, which has been discussed in Ref [3]-[12]. The extensive use of non-renewable energy resource like coal generated toxic environmental conditions. It raised the environmental temperature and caused floods and droughts on earth. So it is genuine to look for the alternative or renewable energy resources to tackle the dangerous results of fossil fuel application. To tackle this problem researchers had put their interest in solar energy exploitation. One such possible solution is photovoltaic application. The major issue in solar cell application is the conversion of light into energy efficiency, cost of the product and environmentally green.

The evolution of solar cells can be divided into four major phases. Among the four major phases perovskite based solar cells are fourth generation solar cells. Perovskite based solar cells successfully produced high power conversion efficiency. Green et al. [13] have published a research on the evolution of solid perovskite solar cell. Kojima et al. [14] reported $CH_3NH_3PbBr_3$ and $CH_3NH_3PbI_3$ compounds as sensitizers in photo electrochemical cells. They successfully acquired photo conversion efficiency of 3.81% for the $CH_3NH_3PbBr_3$ and 3.13% for the $CH_3NH_3PbI_3$ respectively. Sang II Seok and his co-researchers [15] reported good results using hybrid halide perovskite solar cells by optimization of the halides in CH_3NH_3 compound.

2.2 DFT background and evolution:

Ab initio simulations has been very popular in scientific research fields. Within first principle calculations quantum mechanical equations for a system ordered or disordered is solved. Actually it results in one limitation which is the calculation time required because of the complex electron-electron interaction terms. In general the first principle calculations are restricted to around 150-200 atoms calculations with most powerful computer clusters. Time by time efficient algorithms are developed and implemented to model the real materials into computational simulations. The major development of first principle calculations took place with development of Hartree-Fock method or using DFT. Thomas [16] and Fermi [17] (1927) introduced a model to calculate the energy of atoms by approximating the distribution of electrons. Though since that time crucial many body electronic interaction was not taken into account. Later, in 1930, Dirac [18] successfully included the many-body exchange and correlation interactions of the electrons and gave the local density approximation functional (LDA) which is still very popular. The Thomas-Fermi-Dirac model that are based on homogeneous electron gas, did not give the precision values in applications. After that Hartree [19] introduced a method to calculate approximate wave functions and energy states for atoms. After some time, students of Hartree, Fock [20] and Slater [21], separately introduced self-consistent

functions which took into account the Pauli exclusion principals and expressed many electron wave function in the form of Slater-determinants. In 1964, Hohenberg and Kohn purposed basic concepts of density functional theory. [22] They used electron density which is much simple parameter than the wave function. A wave function has 3N variables, where N is the number of electrons in the system and each electron has 3 degrees of freedom. In opposite to that electron density n(r) contains only 3 degree of freedom. Therefore, it was much easier to use electron density than complex wave function. Further Hohenberg and Kohn introduced that all the ground state properties of a material, in particular the ground state total energy, is a unique functional of the ground state density $n_o(r)$ alone. After that Kohn and Sham [23] (1965) proposed a formulation by partially going back to a wave function description in terms of orbitals of independent atomic particles. The main idea was that the many-body problem can be mapped onto a fictitious system of non-interacting atomic particles. Thus a problem of multi electron system is converted into a fictitious non-interacting system having some effective potential. The electron-ion potential and the exchange-correlation potential is included in this effective potential. Modern DFT of today used the same Kohn-Sham based equations to do the calculations.

2.3 DFT study of perovskites:

The theoretical investigation on perovskite material have not kept pace in comparison to experimental studies on perovskite materials. First-principle DFT calculation is a theoretical modelling method used to study the electronic structure of multi-body systems. By using density functional theory properties of multi-body systems are calculated using different approximations for exchange-correlation functional.

Here I reviewed some of the DFT researches that are done on perovskite materials.

Chang et al. [24] used local density functional as an exchange correlation functional to study cubic phase $CsPbX_3$ and $CH_3NH_3PbX_3$ (X = Cl, Br, I), and established the excitonic effective mass comparison.

Borriello et al. [25] applied generalized gradient functional to study the organic-inorganic mixed perovskite based on tin halide and surprisingly deduced that the cation is strongly responsible for the distortion of the perovskite crystal structure.

Recently, due to increase in the theoretical algorithmic developments and more efficient modelling methods, many computational study on halide perovskites structural and electronic properties are reported. [26–35] Different computational methods have been implemented using different exchange-correlation functional such as local density approximation, generalised gradient approximation, and hybrid functional methods etc. Another series of corrections have been implemented to model much real non-covalent interactions like Vander walls corrections and spin orbit considerations.

Geng et al. [36] performed DFT study on Methyl Ammonium Lead Iodide ($MAPbI_3$) perovskite using VASP code by PAW method. They used 4 x 4 x 4 uniform k-mesh for k-space (Brillouin zone) integration. The conjugant-gradient (CG) algorithm based geometry optimization was done with energy convergence criteria of 1×10^{-4} eV with and without implementation of van der walls correction. They implemented PBE exchange functional along with the non-local vdW (van der wall correction) density functional. They found that the orthorhombic structure was the most stable structure for lead iodide perovskite with cell parameters 9.07, 8.77, and 12.80 Å with no vdW correction. They successfully acquired the PbI_6 octahedron tilting with phase transformation from tetragonal to orthorhombic. With vdW correction, the cell parameters resulted are 8.94, 8.94, and 12.98 Å which is lower than the reported data from PBE functional as PBE overestimates the results. The band gap calculated was found to be 1.60 eV compared to the experimental result of 1.63 eV. To understand the electronic structure, projected density of states (PDOS) were also calculated. It revealed that valence band (VBM) for each system is contributed by p electronic state of iodine atom, partly contributed by the s state of lead atom and conduction band maximum is dominated by p-orbital of the lead atom.

Lang et al. [37] investigated ABX_3 cubic (A=Cs, MA; B=Pb; X=I, Br, Cl) perovskites electronic properties using first principle DFT. They considered cubic phase for the calculation and used VASP code with PAW pseudopotential and plane wave basis set implementation. The geometry optimization was done using 8 x 8 x 8 uniform k-mesh and force convergence criterion of 0.01 eV/Å. The generalized gradient functional (GGA) of PBE type was used as an exchange correlation functional for the geometry optimization and HSE functional was utilized for the electronic structure calculation. All the compounds showed very similar electronic properties, having direct band gap at R point of the Brillouin zone, the valence band maximum corresponding to the hybridized state of B-s-X-p orbitals and conduction band maximum corresponding to the p states of the B atoms. The energy band gap values obtained were 3.08, 2.61, and 2.10 eV for $MAPbX_3$ (Cl, Br, I); 2.92, 2.41, and 2.00 eV for $CsPbX_3$ (X=Cl, Br, I) respectively. The dependence of each element on band gap value is verified.

Mosconi et al. [38] performed DFT calculation on tetragonal ABX_3 (X=Cl, Br, I) material using plane wave self-consistent field code as implemented in Quantum-Espresso program package. A 4 x 4 x 4 uniform k-mesh is used for Brillouin zone sampling in the geometry optimization using PBE exchange correlation functional. The optimized cell parameters were 8.78, 8.75, 12.70 Å; 8.29, 8.28, 11.89Å; 7.85, 8.22, 11.15Å for X=I, Br, and Cl respectively. The calculated band gap values were 1.68, 2.07, and 2.57 eV for X=I, Br, Cl respectively. The PDOS calculation revealed the p-X orbital dominance in VBM and p-Pb orbital dominance in CBM satisfying the upward shift of VBM from Cl to I.

CHAPTER – 3

DENSITY FUNCTIONAL THEORY (DFT)

3 Density Functional Theory

The state of a particle is described by its wave function as it contains all information about the particle's state. The wave function of a system is given by Schrodinger wave equation. The time independent Schrodinger equation of a quasiparticle under the influence of the Coulomb potential is given by,

$$\left[-\frac{\hbar^2}{2m}\nabla^2 + V(r)\right]\psi(r) = i\hbar\psi = E\psi(r)$$

Here V(r) is external potential, ψ(r) is quantum state of particle, and E is energy eigen value.

For a system having N number of electrons and M number of atoms, the time independent Schrodinger equation becomes,

$$\left[-\sum_i\left(\frac{\hbar^2}{2M_i}\nabla_i^2\right) - \sum_j\left(\frac{\hbar^2}{2m_e}\nabla_j^2\right) + \left(\frac{1}{2}\right)\sum_{i,j}\left(\frac{Ze^2}{4\pi\varepsilon_o}\right)\frac{1}{|r_j - R_i|} + \left(\frac{1}{2}\right)\sum_{i!=j}\left(\frac{e^2}{4\pi\varepsilon_o}\right)\frac{1}{|r_i - r_j|} + \left(\frac{1}{2}\right)\sum_{i!=j}\left(\frac{e^2}{4\pi\varepsilon_o}\right)\frac{1}{|R_i - R_j|}\right]\psi(r) = E\psi(r)$$

$$H\psi(r) = E\psi(r)$$

Here Hamiltonian (H) operator represents total energy i.e. total potential energy and total kinetic energy of the system. 'E' represents the energy Eigen value, 'Z' is the charges of the individual particles in system and 'ψ' is N-body wave function. By solving above Eigen value equation, one can calculate the possible energy states and corresponding energy Eigen values. The first two expressions in the equation are kinetic energy terms for 'M' number of nuclei and 'N' number of electrons, remaining terms are potential energy between electron and nuclei; electron and electron; nuclei and nuclei respectively.

Since the number of spatial variables depends upon the 3(N+M) degree of freedom, the calculation for the wave function from this equation straightforward is almost impossible/complex for a many body system. The alternate to simplify the cost of the computation is introduced by the Kohn and Hohenberg. They proved that electron probability density alone contains the information about ground state wave function of the system and its properties. Also the electron density has only 3 degree of variable, hence the cost of computation is very low.

3.1 Born-Oppenheimer Approximation

According to this approximation, there is always some momentum transfer between the electrons and ions in an interacting system of nuclei and interacting electrons. It happens due to the large difference in their masses. The forces between the particles are of same magnitude due to their equal charge. So the nuclei should have smaller velocity as it has large mass following the conservation of momentum theorem. On

contrary to that electrons should be more dynamic than nuclei. So we can assume nucleus to be in rest to a ground state in reference to the electron making Hamiltonian term with nuclei fixed. This difference in the nuclear and electronic velocities imparts as separate degree of freedom for nuclei and electron. This approximation is referred as Born Oppenheimer approximation. [39]

$$\sum_i -\frac{\hbar^2}{2M} \nabla_i^2 \quad \text{is neglected}$$

And,

$$\psi_{system} = \psi_{nucleus}(R)\, \psi_{electron}(r)$$

This is the Born-Oppenheimer approximation. According to Hellmann-Feynman theorem, [40]

$$\frac{\partial E}{\partial R} = < \psi_R \left| \frac{\partial H}{\partial R} \right| \psi_R >$$

It allows for the calculation of equilibrium nuclear coordinates where forces on nuclei due to electrons and other nuclei vanishes. This theorem is sufficient to solve the dynamics of nuclei by classical mechanics. A simpler expression for the multi-body Hamiltonian can be defined as,

$$H = -\sum_i \frac{1}{2} \nabla_i^2 + \sum_i \sum_j \frac{Z_j}{|r_i - R_j|} + \frac{1}{2} \sum_i \sum_{k!=i} \frac{1}{|r_i - r_k|} + \frac{1}{2} \sum_l \sum_{m!=l} \frac{Z_j Z_m}{|R_j - R_m|}$$

Here the terms in the above equation are N number of electrons having charge -1 at position 'r_i' and nuclei of charge Z_j at position R_j. No analytic solution is available for materials having multi-body configuration. Here simplified equation is converted into atomic units ($e=m_e=\hbar=4\pi\varepsilon_o=1$) which is more convenient to read for quantum mechanical problems.

3.2 Hartree Method

The simplest approximation for many body system is the Hartree approximation. It says that wave function of all the electrons can be expressed as product of their individual wave functions. [19]

$$\psi(r_1, r_2, .., r_N) = \psi_1(r_1)\, \psi_2(r_2) \ldots \psi_N(r_N)$$

It follows that electrons are independent and interact with only average coulomb potential (Mean field potential). This results in the single electron Schrodinger equations of the form,

$$-\sum_i \left(\frac{\hbar^2}{2m_e} \right) \nabla_i^2 \psi_i(r) + V(r)\psi_i(r) = \varepsilon_i \psi_i(r)$$

Here V(r) is the total potential which includes both nuclear - electron interaction and mean field potential,

$$V_{nucleus-electron}(r) = -Ze^2 \sum_R \frac{1}{|r-R|}$$

$$V_{electron}(r) = -e \int dr' \frac{\rho(r')}{|r-r'|}$$

Where $\rho(r) = \Sigma_i^{occupied} |\psi(r)|^2$

The summation over all the occupied states gives the total electron density.

To calculate the wave function from the Schrodinger equation, we need to determine the Hamiltonian but the Hamiltonian is itself constituted of total kinetic energy and potential energy which is itself depends upon the spatial variable i.e. position of electrons. Since the location of the electrons is not known, we can't write the Hamiltonian term. We want to solve the Schrodinger equation for an electron moving in the potential of the nucleus and all other electrons. So we guess an initial wave function and calculate the electron density. Then use the electron density to write potential energy and kinetic energy forming Hamiltonian. After that solve the Schrodinger equation and again calculate electron density using resultant wave function using $|\psi(r)|^2$. Use this updated electron density to calculate Hamiltonian again and again iteratively until the electron density is converged. This method is called Self consistent field (SCF) approach. [41]

This is very much similar to variational method in which an initial wave function satisfying all known properties is guessed and using that wave function energy is minimized to calculate the ground state energy and wave function.

3.3 Hartree-Fock Method

Hartree method did not satisfy the antisymmetric property of wave function and Pauli's exclusion theorem stating that no two electron can have the same state. Fock improved the Hartree method and introduced Hartree - Fock approximation. [20] In Hartree - Fock approximation, wave function is changed on interchange of any two electron position and it follows,

$$\psi(r_1, r_2, \dots, r_N) = -\psi(r_1, r_3, r_2 \dots, r_N)$$

Here r_i includes position and spin coordinates. The wave function is represented by antisymmetric single slater determinant of wave function for single particle which satisfies the anti-symmetricity and normalised.

$$\psi(r_1, r_2, \dots, r_N) = \frac{1}{\sqrt{N}} |\psi(r_1)\psi(r_2) \dots \psi(r_N)| = \frac{1}{\sqrt{N}} D$$

$$D = \Delta \begin{pmatrix} \psi_1(r_1) & \psi_1(r_2) \cdots & \psi_1(r_N) \\ \vdots & \psi_i(r_2) & \vdots \\ \psi_N(r_1) & \psi_N(r_2) \cdots & \psi_N(r_N) \end{pmatrix}$$

Here $\psi_i(r_j)$ are one-electron wave functions. This antisymmetric wave function is inserted into the Hamiltonian expression and the total energy is calculated. Any non-singular transformation cannot change the determinant value, we can take orthonormal set of ψ. To normalise the wave function, Lagrange multiplier ε_i is introduced and minimising it with respect to ψ,

$$\frac{d}{d\psi}\left[< H > - \sum_j \varepsilon_j \int |\psi_j|^2 \, d\boldsymbol{r}\right] = 0$$

Finally above equation reduces to one-electron Hartree-Fock equations of the form,

$$-\frac{\hbar^2}{2m} \nabla^2 \psi_i(r) + V_{nucleus}(r)\psi_i(r) + U(r)\psi_i(r) = \varepsilon_i \psi_i$$

Here U(r) is a special potential and the local external potential is denoted by $V_{nucleus}$. The full Hartree-Fock expression is given by,

$$-\frac{\hbar^2}{2m} \nabla^2 \psi_i(r) + V_{nucleus}(r)\psi_i(r) + \sum_j \frac{\int dr' |\psi_j(r')|^2}{|r - r'|}\psi_i(r) - \frac{\Sigma_j \int dr' \psi_j^*(r')\psi_i^*(r')\psi_j(r)}{|r - r'|} = \varepsilon_i \psi_i(r)$$

Here the first term is the kinetic energy of electrons, second term is electron - ion interaction potential, third term is electrostatic potential from N electronic charge distribution which comprises self-interaction of electrons with their own when i=j. The exchange term act only on electrons with same spin and having anti-symmetric wave function. The physical meaning of exchange is to avoid like-spin electrons and fourth term is exchange term.

3.4 Thomas-Fermi Approximation

Thomas-Fermi Approximation is a precursor theory to modern density functional theory. The Thomas-Fermi theory relates the K.E. of non-interacting homogenous gas with charge density in the form of a functional having some external potential V(r) which is itself a function of charge density. [42] This is a local density functional and based on a semi classical approximation. This formulation becomes exact for the uniform electron gas. This Thomas-Fermi model is widely used in the current modern DFT.

Generally electrons are distributed non-uniformly inside an atom. In T-F model, an approximation is used that the electrons are distributed uniformly in small volumes and the electron density can change form one small volume to another. The kinetic energy in

the form of charge density functional can be derived by integrating the phase space volumes and leads to following expression,

$$T = C_{kinetic} \int [n(r)]^{\frac{5}{3}} d^3r$$

Where $C_{kinetic}$ is given by,

$$C_{kinetic} = \frac{3h^2}{40m_e} \left(\frac{3}{\pi}\right)^{\frac{2}{3}}$$

So according to the Thomas-Fermi approximation, kinetic energy can be expressed in terms of density. Though the Thomas-Fermi model is not accurate because of the approximation used. Many researchers improved this model and gave a correction in the model like Thomas-Fermi-Dirac model etc. [43] However Kohn and Sham introduced the fictitious non-interacting system that cancelled the problem to some extent the problem.

3.5 Modern Density Functional Theory (DFT)

DFT uses the electron density as main parameter instead of using the old wave function approach. This difference results in a significant reduction in complexity i.e. decreasing the cost of the computation. It happens because density is a function of three coordinate direction in comparison to 3N degree of freedom dependence for the full many-body wave function. This theory is different from other computational method in the manner that it does not results in a correlated multi-body wave function. Density functional theory uses the functional dependence over density for the Hamiltonian term. DFT has a potential of very calculating very accurate results at comparatively low time cost.

3.5.1 Hohenberg-Kohn (H-K) Theorems

DFT was put on a solid theoretical footing by the two H-K theorems. [44] These theorems are as follows,

"The external potential is a unique functional of the electron density n(r) only. So the Hamiltonian and thereby all the ground state properties like energy and wave functions can be determined by density of electron alone."

Define a functional F[n(r)] such that,

$$F[n(r)] = < \psi | T + V_{e-e} | \psi >$$

Here T is the kinetic energy and $V_{e\text{-}e}$ is the interaction between electron and electron. F[n(r)] is termed as universal functional because it has the dependence only on the electron density, n(r) of any system, not on external potential.

The energy functional E[n(r)] can be written as,

$$E[n(r)] = F[n(r)] + \int dr\, n(r)v(r)$$

Here F[n(r)] is universal functional depending on electron density which is unknown. We can write the expression of energy as,

$$E[n(r)] = < \psi|H|\psi >$$

So the Hamiltonian is given by,

$$H = F + V$$

Where V is the external potential operator, and F is the electronic Hamiltonian (F = T + $V_{e\text{-}e}$). To prove the above statement consider two potentials $v_1(r)$ and $v_2(r)$ which differ by some constant and these two different potential lead to two different ground state wave functions $\psi_1(r)$ and $\psi_2(r)$. Assuming that these two gives the same ground state charge density n(r), then according to variational principle,

$$E_1 \leq < \psi_2|H_1|\psi_2 > = < \psi_2|H_2|\psi_2 > + \psi_2|H_1 - H_2|\psi_2$$

$$= E_2 + \int n(r)[v_1(r) - v_2(r)]dr$$

After interchanging E_1 and E_2, results similar expression, and after adding the both expression meets the following contradiction in the statements,

$$E_1 + E_2 \leq E_1 + E_2$$

"The ground state energy can be obtained variationally i.e. the density that minimises the energy is the exact ground state energy."

The Hohenberg-Kohn theorems are the building blocks of DFT. The Hohenberg-Kohn stated that the ground state electron density $n_o(r)$ minimizes the energy functional E[n],

$$E[n] = F[n] + \int n(r)V_{ext}(r)dr \quad \ldots(1)$$

Where F[n] is universal functional of n(r) and the minimum value of functional E[n] is E_o i.e. the exact ground-state energy. To prove the above H-K statement, assume a density functional G defined by,

$$G[n(r)] = \min_{\psi \to n(r)} < \psi|G|\psi >$$

Here bracket term is found by taking all wave functions ψ, putting density n(r) and then selecting the wave function which further minimizes G. F[n] in above theorem is represented by,

$$F[n(r)] = \min_{\psi \to n(r)} < \psi|F|\psi >$$

So that,

$$F = \sum_i -\left(\frac{1}{2}\right)\nabla_i^2 + \left(\frac{1}{2}\right)\sum_{i!=j}\left(\frac{1}{|r_i - r_j|}\right)$$

Assuming an N-electron ground state wave function ψ_o which gives the electron density n(r) and minimises $<\psi|F|\psi>$, from previous energy functional,

$$E[n(r)] = F[n(r)] + \int n(r)V_{ext}(r)dr = <\psi|F + V_{ext}|\psi>$$

In above equation Hamiltonian is comprised of $F+V_{ext}$, and that is why E[n(r)] should follow variational principle, which states

$$E[n(r)] \geq E_o \qquad \ldots(2)$$

Which means the Energy functional E[n(r)] gets from the first Hohenberg-Kohn theorem has a lower bound. So from equation (1), we can say

$$F[n_o(r)] \leq <\psi_o|F|\psi_o>$$

Since ψ_o is a dummy wave function yielding $n_o(r)$. Then after summing up the above equations,

$$E[n_o(r)] \leq E_o \qquad \ldots(3)$$

And equation (2) and (3) implies that,

$$E[n_o(r)] = E_o$$

Although Hohenberg-Kohn theorems proved the existence of such universal functional, but the nature of the functional and about the calculation of the ground state density is not given. This is successfully done by the Kohn-Sham DFT formulation which is the modern DFT.

3.5.2 Kohn-Sham DFT Theory

Kohn-Sham DFT is based on the trick where we consider a fictitious non-interacting system having the same number of electrons as interacting one with same effective potential, called Kohn-Sham potential $V_{ks}(r)$. [23] The Kohn-Sham orbitals of individual particles are restricted to yield the same ground state density as that of the fully interacting system, so in a way H-K and Kohn-Sham theorems do hold true and apply here. The constrained of fixed number of electrons can be represented by,

$$\int n(r)dr = N$$

The change in the total energy functional E[n] with respect to electron density n(r) under fixed number of electron constrained gives,

$$\frac{\partial}{\partial n(r)}\left[F[n(r)] + \int v_{ext}(r)n(r)dr - \mu\left(\int n(r)dr - N\right)\right] = 0$$

Where μ is Lagrange multiplier having some constraint. This constraint is about the fixed number of electrons in the system. The Euler-Lagrange combined within minimisation of this functional represents,

$$\mu = \frac{\partial F[n(r)]}{\partial n(r)} + v_{ext}$$

The Kohn-Sham derivation allow us to write universal functional F[n(r)] by,

$$F[n(r)] = T_s[n(r)] = E_H[n(r)] + E_{xc}[n(r)]$$

Here the term $T_s[n(r)]$ is the K.E. which can be written in terms of non-interacting quasiparticles states as

$$T_s[n(r)] = -\frac{1}{2}\sum_{i}^{N} \psi_i^*(r)\,\nabla^2\psi_i(r)dr$$

The important thing to notice here is that the kinetic energy mentioned above is not actual interacting system kinetic energy, but it is a kinetic energy of the fictitious non-interacting system taken. $E_H[n(r)]$ is the Hartree potential functional that represents the interaction potential on an electron due to other electrons taken mean of them altogether. Hartree potential incudes self-interaction term as well. Hartree potential functional is given by, [45]

$$E_H[n(r)] = \frac{1}{2}\int\int \frac{n(r)n(r')}{|r-r'|}\,dr\,dr'$$

The Euler-Lagrange equation is written as,

$$\mu = \frac{\partial T_s[n(r)]}{\partial n(r)} + V_{ks}(r)$$

Here V_{ks} is the effective Kohn-Sham potential and given by,

$$V_{ks}(r) = V_{ext}(r) + V_H(r) + V_{xc}(r)$$

Here Hartree potential (V_H) is given by,

$$V_H(r) = \frac{\partial E_H[n(r)]}{\partial n(r)} = \int\left(\frac{n(r')}{|r-r'|}\right)dr'$$

And V_{xc} is exchange-correlation potential,

$$V_{xc}(r) = \frac{\partial E_{xc}[n(r)]}{\partial n(r)}$$

After all these formulations, now the Hartree equation shares the form as of Euler-Lagrange equations. Therefore we can evaluate it just like Schrodinger based equations of the form,

$$\left(-\frac{1}{2}\nabla^2 + V_{ks}(r)\right)\psi_i(r) = \varepsilon_i\psi_i(r)$$

Where ε_i represents the energy Eigen values of the single particle wave function and electron probability density n(r) is formed by the Kohn-Sham orbitals as follow,

$$n(r) = \sum_{i=1}^{N} \psi_i^*(r)\,\psi_i(r)$$

A slater determinant of Kohn-Sham states can form the many-body wave function. Hence Kohn-Sham formulation succeeds in transforming the N-body problem into N single body problems, each joined by the Kohn-Sham potential. Kohn-Sham eigen values are just created to help in determination of the ground state density $n_o(r)$. Exception is the eigenvalue of the highest occupied state as it represents the ionisation energy of the system. The above equations can calculate very accurate ground state energy provided the more accurate exchange correlation functional E_{xc}. The exact value of E_{xc} is not known and its form can be approximated with the type of approximation and the level of accuracy in this approximation determines the accuracy of the calculation.

3.6 Exchange-Correlation Interaction

The Kohn-Sham equations mentioned since now are exact and no approximations have been made, throughout the theory in this thesis we mapped the actual interacting system with a fictitious non-interacting system that gives the same ground state density. But as showed earlier, the Kohn-Sham kinetic energy is not the actual kinetic energy of the actual system. So we can use it to define the exchange-correlation energy as follows,

$$E_{xc}[n(r)] = T[n(r)] - T_s[n(r)] + E_{ee}[n(r)] - E_H[n(r)]$$

Where $T_s[n(r)]$ and $E_{ee}[n(r)]$ are the exact kinetic energy functional and electron-electron interaction energy functional respectively. Physically the exchange-correlation can be interpreted as containing the contributions of detailed correlation and exchange to the system energy. We can compute every piece of a Kohn-Sham DFT energy exactly except for the "exchange-correlation energy functional ($E_{xc}[n(r)]$)". There is no absolute value for exchange correlation functional, the accuracy of the DFT depends upon the exchange correlation functional approximation. There are many exchange correlation functional

developed so far by researchers. Commonly used and most popular of them are described below as following,

3.6.1 Local Density Approximation (LDA)

Local Density Approximation assumes that the exchange-correlation energy at a point r is simply equal to the exchange-correlation energy of a uniform electron gas having same electron density at the point r. [46] In the local density approximation (LDA), the value of exchange-correlation energy of an electron in a homogenous electron gas of the same density n(r) is,

$$E_{XC}^{LDA}[n(\boldsymbol{r})] = \int \varepsilon_{XC}\big(n(r)\big)\, n(\boldsymbol{r}) d\boldsymbol{r}$$

The value of exchange-correlation potential is written as,

$$v_{xc}(r) = \frac{\partial E_{xc}[n(r)]}{\partial n(r)} = \frac{\partial\big[n(r)\varepsilon_{xc}\big(n(r)\big)\big]}{\partial n(r)}$$

The most accurate data for ε_{xc} can be calculated from QMC calculations. The local density approximation is surprisingly accurate for metals and for systems in which density don't vary too much it gives good results. Also the failings of LDA is also very well known, it over-binds molecules and solids, and generally favours the homogenous systems.

3.6.2 Generalised Gradient Approximation (GGA)

The GGA tries to incorporate the effects of inhomogeneities by adding the gradient term of the electron density (∇n(r)). [47] The expression for GGA exchange-correlation functional is given by

$$E_{xc}^{GGA}[n(r)] = \int n(r)\ \varepsilon_{xc}^{hom}[n(r)] F_{xc}[n(r), \nabla n(r)] dr$$

There is no unique form of GGA unlike LDA, as the change in the form of ∇n(r) and F_{xc}, many possible variations are possible for GGA exchange correlation functional. Most popular of them are PBE, PW91 functional. The GGA succeeded in reducing the effects of over binding due to LDA and more successful when applied to molecules and non-metals.

3.6.3 Hybrid Functional

Hybrid Functional is an approximation for the exchange correlation energy functional in DFT which includes a part of exact exchange term from Hartree-Fock theory and rest part of the exchange-correlation from the other sources like first principle methods having some respective weights. The E_{XC} part is expressed in terms of K-S states instead of electron density. In 1993, Axel Becke introduced this hybrid method for implementing density functional approximations. Application of hybrid functional improves the accuracy of molecular properties, such as bond length, lattice energies, and vibrational frequency. Mostly used Hybrid functional are B3LYP, HSE etc. [48]

For B3LYP, the exchange-correlation functional energy is given by,

$$E_{xc}^{B3LYP} = E_x^{LDA} + a_o(E_x^{HF} - E_x^{LDA}) + a_x\,(E_x^{GGA} - E_x^{LDA}) + E_c^{LDA} + a_c(E_c^{GGA} - E_c^{LDA})$$

Here a_o=0.20, a_x=0.72, a_c=0.81 and E_x^{GGA}, E_c^{GGA} are generalized gradient approximations respectively.

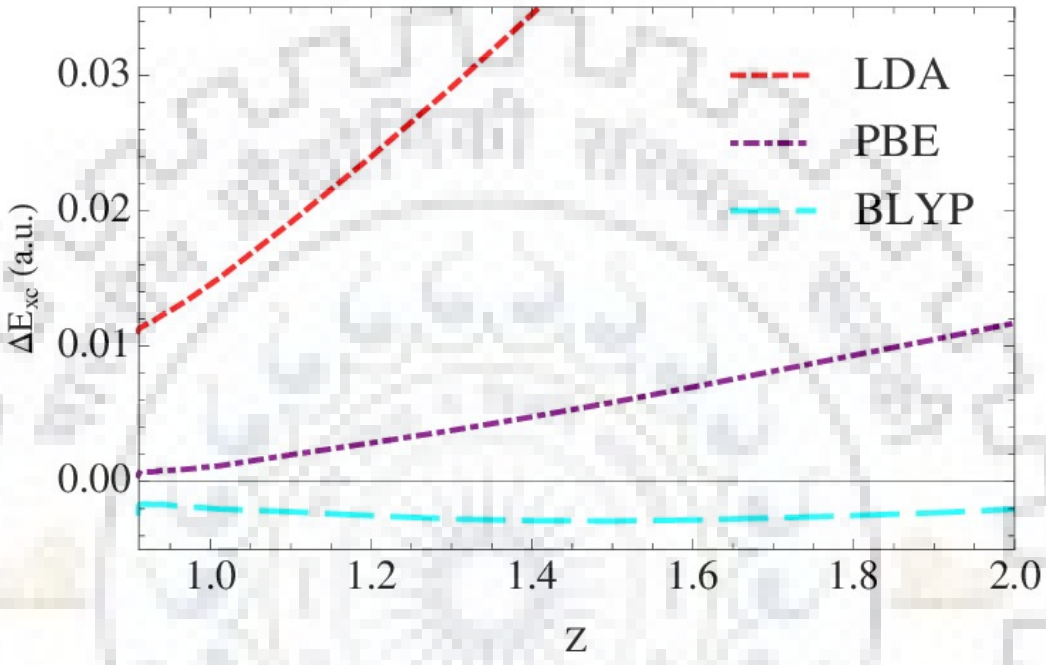

Figure 3.1: Error in exchange-correlation energy with exchange-correlation approximations, Taken with permission from Ref [49]

For some materials the error associated with calculated electronic properties was found to be very significant. One such material was the Mott's insulator for which LDA and GGA described it as a metal but in real it was insulator. This error was explained by strong correlations between localised electrons of the material.

3.6.4 DFT+U method

DFT+U method is inspired from Hubbard model. For materials having strong correlations between the electrons like in Mott insulators, exact Hartree-Fock equations fail to predict correctly. In these Mott insulators, band gap is the result of competition between the coulomb potential U between 3d electrons and the transfer integral t of the tight-binding approximation of 3d electrons between neighbouring atoms. [50] So the bandgap can be described by the parameter U, t and z term that denote the number of nearest neighbour atoms,

$$E_{gap} = U - 2zt$$

To relieve this problem, DFT+U correction has been implemented using U correction (Hubbard parameter) in new Hamiltonian that take cares of electron correlations of that 3d orbital. It predicts accurate physical properties, electronic properties, intermolecular interactions and formation energies with considerably lower computational cost.

3.7 Self-Consistent Field Approach

To calculate the ground state wave electron density from the Kohn-Sham equations, we need to determine the Hamiltonian but the Hamiltonian is made up of total kinetic and potential energy which is itself depends upon the spatial variable i.e. position of electrons. Since we don't know the location of the electrons we can't write the Hamiltonian. We want to solve the set of Kohn-Sham equations for an electron moving in the potential of the nucleus and all other electrons. So we guess an initial wave function and calculate the electron density. This initial guess of electron density is formulated by implementing plane wave basis set $\{\psi_i\}$, which is given by,

$$\psi_k(r) = \sum_i c_{ki}\, \Phi_i(r)$$

Since plane waves can be infinite in number to represent an accurate wave function in basis set, a cut-off needs to be used to limit the computation reach infinity. The restriction is provided by kinetic energy cut-off for electric density that is explained in next section. Then use the electron density to write potential energy and kinetic energy. After that solve the Kohn-Sham equation and again calculate electron density using resultant wave function using $|\psi(r)|^2$. Use this updated electron density to calculate Hamiltonian again and again iteratively until the electron density is converged. This method is called Self consistent field (SCF) approach. [41] A simple schematic of the self-consistent approach is as following,

Schematic diagram of self-consistent approach

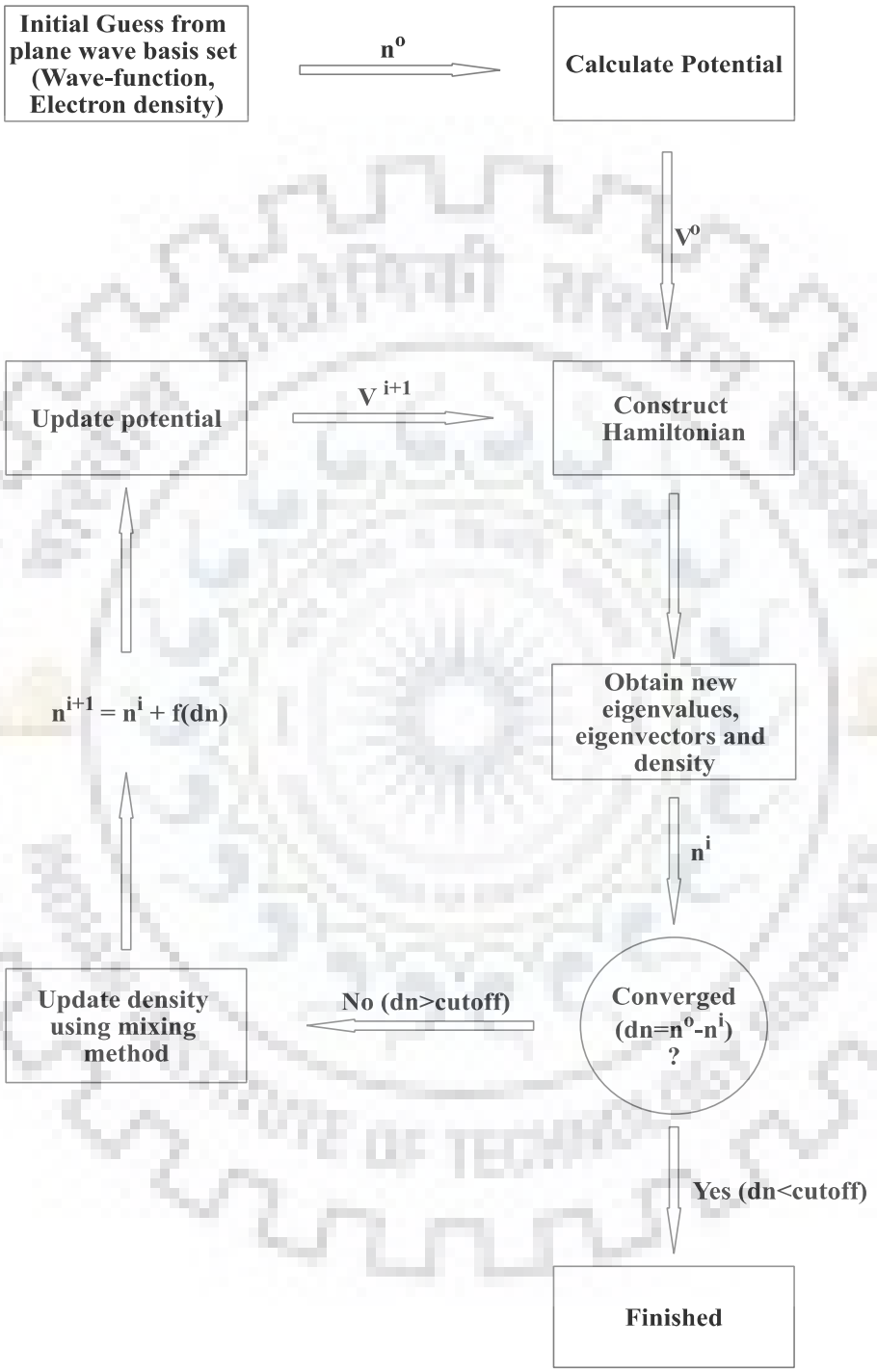

Figure 3.2: Schematic of self-consistent field method

CHAPTER – 4

DFT COMPUTATIONAL DETAILS

4 Computational Details

In this dissertation work optimization of crystal structure, electronic properties like energy band gap values, and elastic properties like bulk modulus has been calculated for $MAPbX_3$ (X=Cl, Br, I). Further two approximation methods have been implemented to show their computational accuracy. All the first principle DFT computations are done using open source Quantum espresso v6.3 package code based on DFT, plane waves and pseudopotentials. Quantum espresso uses FORTRAN compiler to compile the q-e code. All calculations are executed on high performance cluster system based on open message parsing interface (open-mpi) services for high performance. We employed orthorhombic, orthorhombic and tetragonal crystal cells with 48 atoms each for $MAPbX_3$ (X=Cl, Br, I) respectively. Electron and ion interactions are described by ultrasoft pseudopotentials with electrons from Pb 5d, 6s, 6p; N and C 2s, 2p; H 1s; I 5s, 5p; Br 4s, 4p; Cl 3s, 3p, orbitals explicitly included in the calculations. Two exchange-correlation functional approximations i.e. local density functional (LDA) and generalized gradient approximations (GGA) is utilized. Scalar relativistic exchange correlation functional constructed by Perdew-Burke-Ernzerhof (PBE) for GGA and Perdew-Zunger (PZ) for LDA has been applied to all constituent atoms. In order to limit plane wave computation reach infinity, kinetic energy cut-off for wave functions and charge density are being calculated by converging total DFT energy. The Brillouin zone sampling is done using Monkhorst-Pack scheme of 8 x 8 x 8 k-point grid (corresponding to 512 k-points) for both structure optimization and electronic structure calculation throughout the materials.

4.1 Plane wave cut-off:

A convergence test for plane wave kinetic energy cut off for wave-function and electron density is applied to restrict computation reach infinity. Convergence has been acquired using plain mixing with successive iterations at only gamma point to reduce the computation time. The convergence criteria for energy convergence is taken as $1x10^{-6}$ Ry as it is the starting level of error that quantum espresso can introduce.

Ecut (Ry)	$MAPbCl_3$		$MAPbBr_3$		$MAPbI_3$	
	LDA	GGA	LDA	GGA	LDA	GGA
Wfc	65	44	65	78	70	80
Rho	380	420	360	500	380	440

Table 4.1: Converged plane wave kinetic energy cut-off values.

Here Ecut Rho is kinetic energy cut-off for electron density and potential; Ecut Wfc is kinetic energy cut off for wave function in Rydberg energy units.

4.2 Structural Optimization:

Variable cell relaxation method has been used to optimize the crystal structures of perovskite material. This method has been instructed to relax the structure by moving all three lattice parameters including angles between them simultaneously throughout the iterations without any constraint. Initial lattice constants and atomic coordinates for all three materials are obtained from single crystal XRD data available in literature. [51] The maximum force tolerance, maximum force on each atom is $1x10^{-3}$ eV/Å during the optimization. All the structures in this study is optimized using bfgs quasi Newtonian algorithm (2nd order). Periodic boundary condition is employed in all the three dimensions. All the structures has successfully optimized within 25-28 bfgs cycles under given convergence criteria. The plots for minimization of force on an atom and stress along a particular direction is represented in results sections for each material. Additionally, the energy minimization is carried by Davidson diagonalization with 25-28 steps and maximum 200 iterations per step.

4.3 Electronic Structure Calculation:

To calculate energy eigen values and wave functions, self-consistent calculation is done using the same energy minimization configuration as in variable cell relaxation i.e. iterative Davidson diagonalization using plane wave basis sets limiting with kinetic energy cut off for wave functions, electron density having energy convergence criteria of $1x10^{-6}$ Ry between two successive iteration. The self-consistent calculation is done on optimized crystal structures. The wave function and energy eigenvalue calculation is carried out for Monkhorst-Pack scheme of 8 x 8 x 8 uniform k-points mesh. Finally energy bands (energy values) are calculated along the most symmetric k-path of the lattice with 20 intermediate k-points along each direction (k-path) using non-self-consistent calculation. The choice of symmetric k-path in Brillouin zone, is carried out by visualising the optimized crystal structure on Xcrysden.

For a better understanding of electronic structure of the perovskite materials, density of states (DOS) and projected DOS have been calculated as well. DOS and PDOS have been calculated using gaussian broadening for a transparent visualization of orbital contributions. To add the respective projected DOS of each orbitals, “sumpdos” feature package is being used.

4.4 Bulk Modulus Calculation:

To calculate the bulk modulus of elasticity of perovskite materials, the calculation of E-V curve using some equation of states is done. In general, bulk modulus B relates the change in volume of a material with a change in pressure (at constant temperature) and given by,

$$B = -V\frac{dP}{dV}$$

Changing all dimensions of crystal cells simultaneously, corresponds to putting positive (negative) pressure on the crystal cell. The pressure change at constant temperature follows from energy change by,

$$P = -\frac{dE}{dV}$$

So bulk modulus B, is

$$B = V_o \frac{d^2E}{dV^2}$$

Where V_o is equilibrium lattice volume.

A set of 11 lattice volume is taken around the optimized equilibrium volume in the range $0.9V_o \leq V \leq 1.1V_o$. All the respective lattice parameters are calculated only varying one lattice parameter from the volume. The DFT energy is calculated for these 11 different lattice configurations, and successfully obtained E-V curve. This E-V curve is fitted into parabola using some equation of states (birch, keane, murnagham) i.e. already included in Quantum espresso "ev.x" package. From the fitted E-V parabola, elastic property bulk modulus is calculated for four equation of states fittings. The typical fitted E-V curve for one such calculation is as follows, (remaining curves are in results chapter)

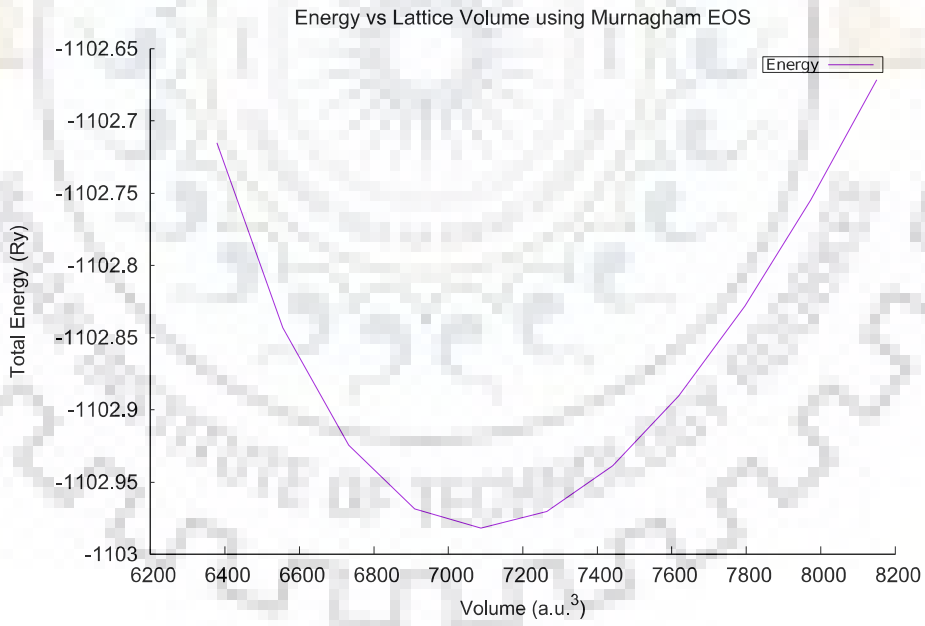

Figure 4.1: E-V curve for $MAPbI_3$ using GGA

CHAPTER – 5

EXPERIMENTAL DETAILS (MATERIALS, METHOD AND RESULTS)

5 Experimental Details

5.1 Materials Used

The synthesis method for perovskite materials has the significant application in determining the morphology of the perovskite films. The additional purity is a plus to achieve high efficiency of the device. Here, methylamine solution (33wt% in ethanol), hydro halide acid (HX) (57wt% in water), and lead halide salts PbX_2, and lead acetate are purchased and used as received. Indium-doped tin oxide (ITO) coated glass substrates are purchased from M/S Global Nanotech. All the other solvents were obtained from the Sigma-Aldrich (St. Louis, MO).

5.2 Perovskite Precursor Synthesis

Three flasks were cleaned well using water bath sonicator. All the three flasks were filled with 50ml of ethanol and 12ml of methylamine (33wt% in ethanol). The reaction was performed at constant 0^oC while the flask was put in a water bath filled with ice and water. 5ml of hydro halide (HX) acid (57% in water) was added drop wise while stirring. The reaction was exothermic and occurred for two hours at 0^oC. The final product formed was recovered with rotary evaporator at 60^oC in 30 minutes to evaporate solvents like ethanol and water. The recovered product was light yellow, it means a small amount of residual is still mixed with ammonium salt. To get more pure product, I washed residual powder with diethyl ether at room temperature for three times. After washing it, a white powder was obtained. The final MAX ammonium salt is dried in the vacuum overnight.

5.3 Perovskite Thin Film Fabrication

First of all, I cleaned the substrate glass slides that were ITO coated using ethanol, acetone, and DI water into water bath sonicator. I used one step method in which I co-dissolved equimolar MAX and PbX_2 (X=I, Br, Cl) into DMF solvent and then the solution was kept in ultrasonic bath for ultra-sonication until solutes were completely dissolved. To coat perovskite thin film onto substrate uniformly, spin coating method was used. A small amount of 100 µl of the prepared solution was dripped dropwise at the centre of the substrate, which was placed firmly on spin coater using vacuum suction. The solution and the substrate were maintained at 70^oC and 60^oC respectively. The whole experiment was carried out in ambient condition with controlled humidity. The substrate was allowed to rotate at 6000 rpm for 30 sec in order to spread the solution uniformly by centrifugal force. After spin coating, the films were annealed on hot plate at 120^oC for 10 minutes and after that fabricated perovskite films were put in the vacuum desiccator as perovskite films are prone to damage in room environment.

5.4 Characterization Techniques

5.4.1 Field Emission Scanning Electron Microscopy (FE-SEM)

For a better topographic details of perovskite films, perovskite film were scanned by FE-SEM. This characterisation technique can provide upto few nanometre range resolution. **Figure 5.1-5.3** represent the FE-SEM images of all three perovskites films namely $CH_3NH_3PbX_3$ (X=I, Br, Cl) revealing very clear topographic picture of the films.

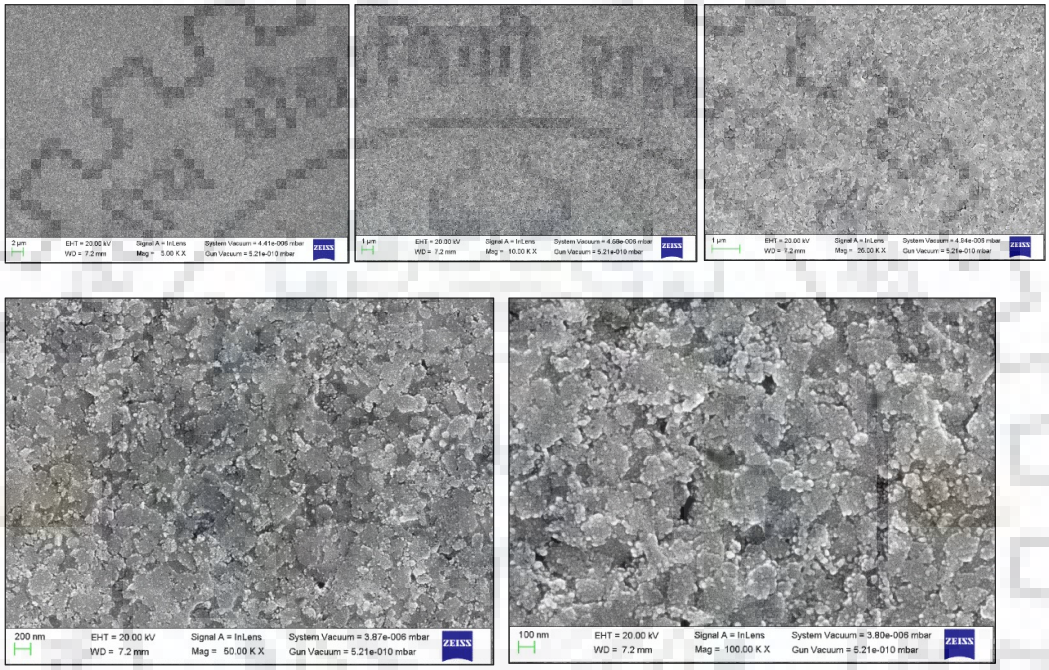

Figure 5.1: FE-SEM image of $MAPbI_3$ film with magnification ranging 5-100 K X.

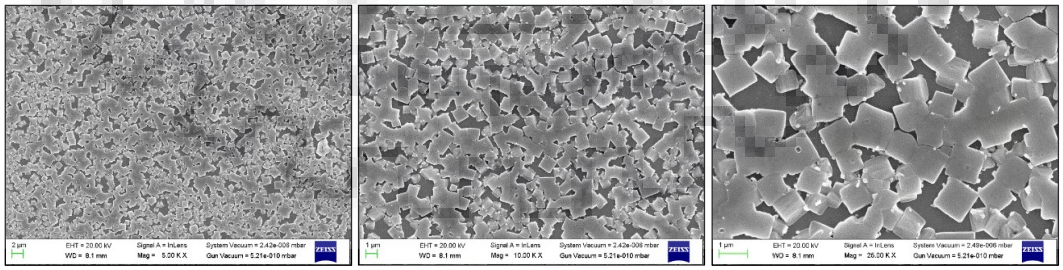

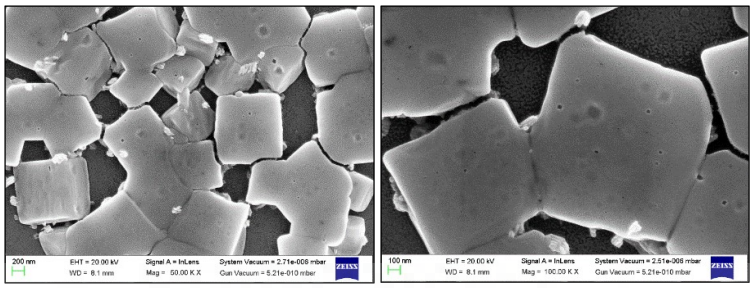

Figure 5.2: FE-SEM image of $MAPbBr_3$ film with magnification ranging 5-100 K X.

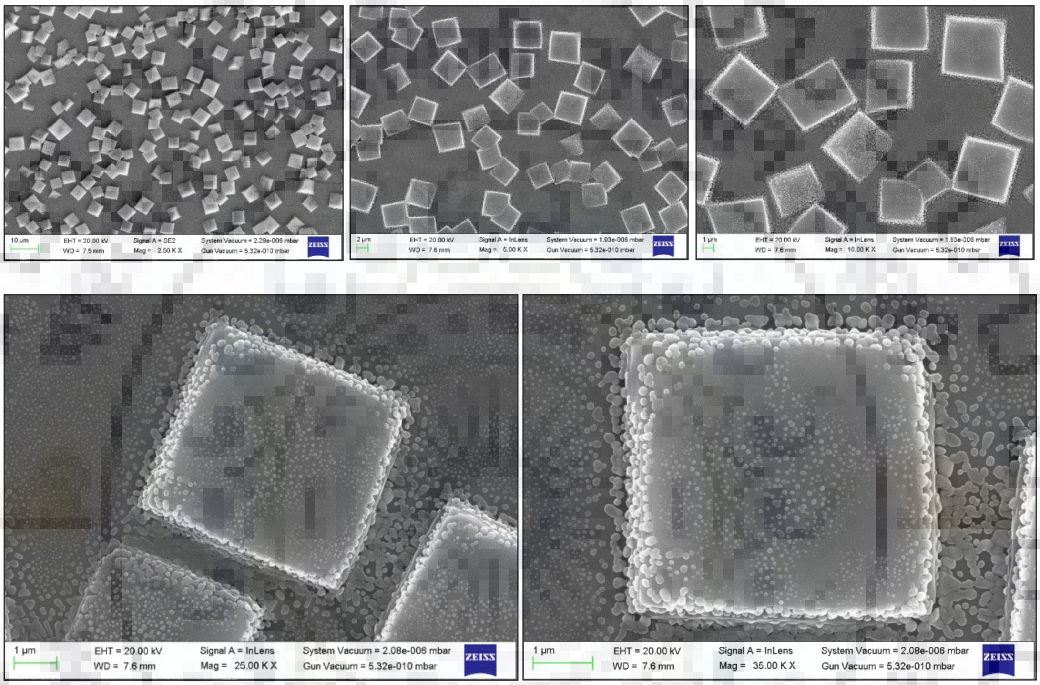

Figure 5.3: FE-SEM image of $MAPbCl_3$ film with magnification from 5 K X to 35 K X.

From above FE-SEM images, all three perovskite thin films topology is clearly visible. We can see the nice crystals formed and the gaps between them. From the above FE-SEM topology, we can see that the gaps between $MAPbCl_3$ crystals is more compared to the $MAPbI_3$ crystals that can be a potential source of weak electronic conductivity.

5.4.2 X-ray Diffraction (XRD)

X-ray diffraction is powerful tool to characterize quality of crystalline materials. XRD measurements are taken to further investigate the formation of perovskite film and crystallization. **Figure 5.4** shows XRD of $CH_3NH_3PbX_3$ (X=I, Br, Cl) perovskite thin films. For comparison, XRD pattern of three perovskite thin films shows that main peaks for the $MAPbI_3$ are at 2θ = 14.17˚, 19.86˚, 28.54˚, 30.4˚, 32.07˚, 50.8˚; for $MAPbBr_3$ at 14.93˚, 21.16˚, 30.43˚, 33.9˚, 35.26˚, 43.12˚, 45.9˚ and for $MAPbCl_3$ at 15.56˚, 31.57˚ and 35.23˚ which is in agreement with the literature.

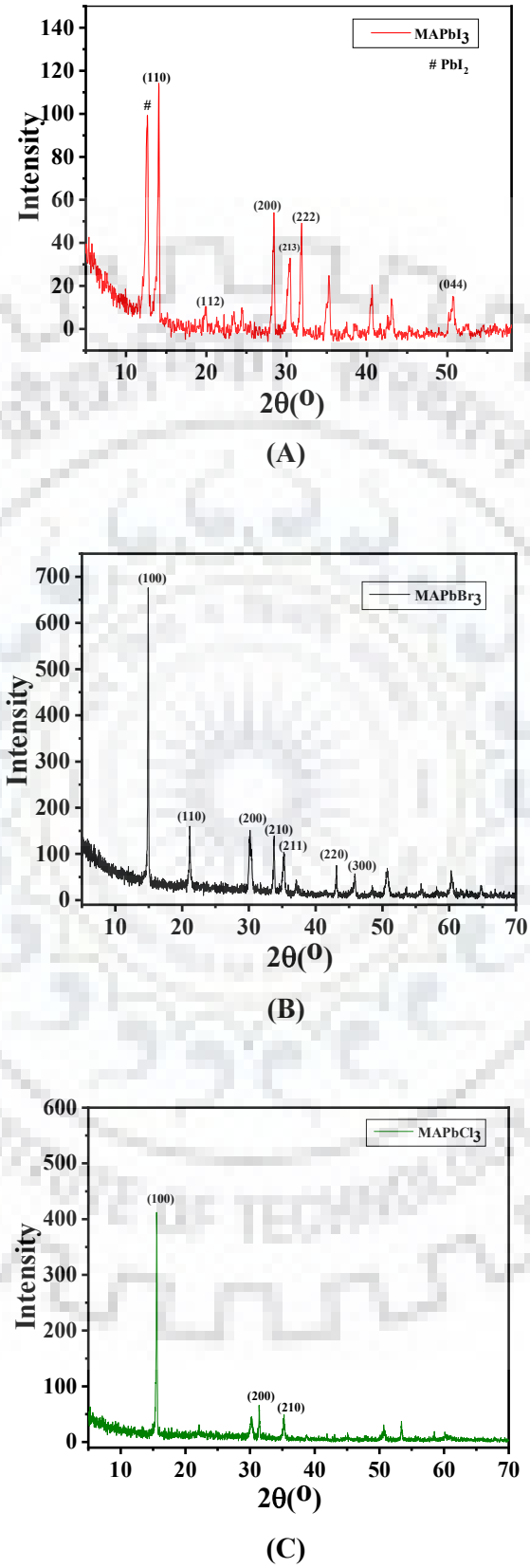

Figure 5.4: Powder XRD pattern of $MAPbX_3$, (A) X=I, (B) X=Br, (C) X=Cl perovskite films.

5.4.3 UV-Visible Technique

The steady state absorption for the perovskite films are shown in the **Figure 5.5**. The UV-visible spectrum represents that the absorption peak occurs around 780, 520, and 420 nm for $MAPbX_3$ (X=I, Br, Cl) respectively. The energy band gap values were obtained by plotting Tauc plot of $(\propto.h.\upsilon)^{1/m}$ against photon energy ($h\upsilon$). As all three $CH_3NH_3PbX_3$ (X=I, Br, Cl) perovskites are direct band-gap semiconductor perovskites, the value of "m" is ½. By extrapolating the linear region of the $(\propto.h.\upsilon)^2$ to the energy axis ($h.\upsilon$) intercept as represented in the right side plot of **Figure 5.5**, energy band-gap (E_g) is established.

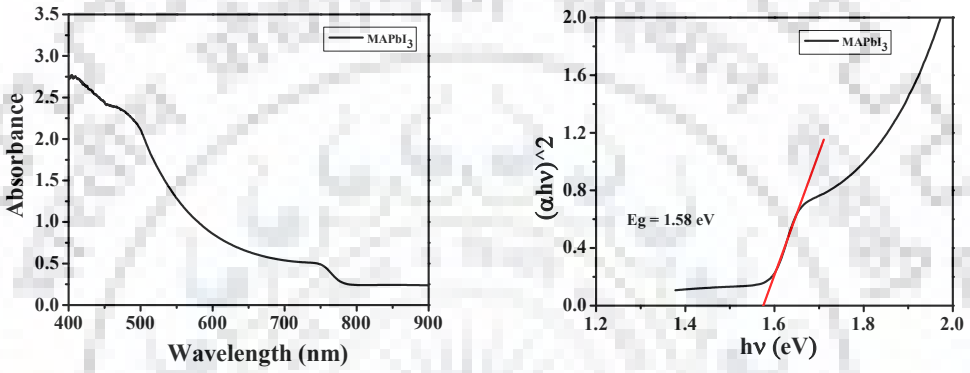

Figure 5.5: (a) UV-vis absorption spectrum (left) and Tauc plot (right) for $MAPbI_3$.

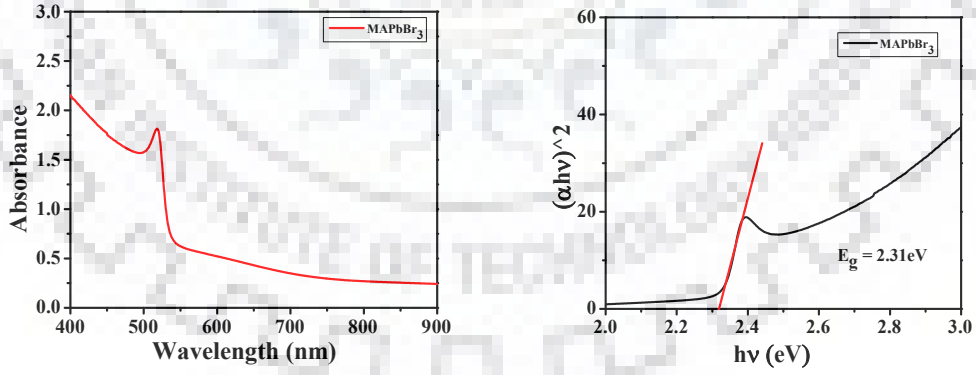

Figure 5.5: (b) UV-vis absorption spectrum (left) and Tauc plot (right) for $MAPbBr_3$.

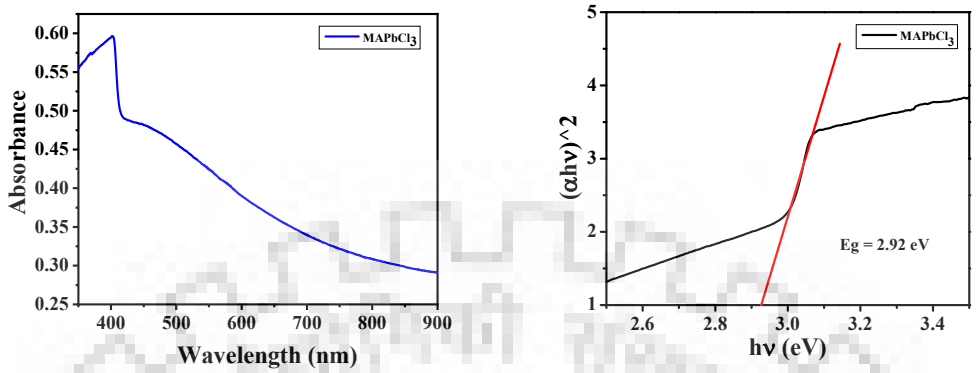

Figure 5.5: (c) UV-vis absorption spectrum (left) and Tauc plot (right) for $MAPbCl_3$.

Film	Ionic Radius of X (Å)	λ (nm)	E_g (eV)
$MAPbI_3$	2.20	780	1.58
$MAPbBr_3$	1.96	520	2.31
$MAPbCl_3$	1.81	420	2.92

Table 5.1: Experimental band-gap values of $MAPbX_3$ (X=I, Br, Cl)

All the energy band gap values acquired form the experiment and Tauc plot strongly in the agreement with the literature band gap values.

CHAPTER – 6

RESULTS AND DISCUSSION

6 Results

6.1 Plane wave kinetic energy cut-off convergence:

Convergence results for Methyl Ammonium Lead Iodide ($MAPbI_3$):

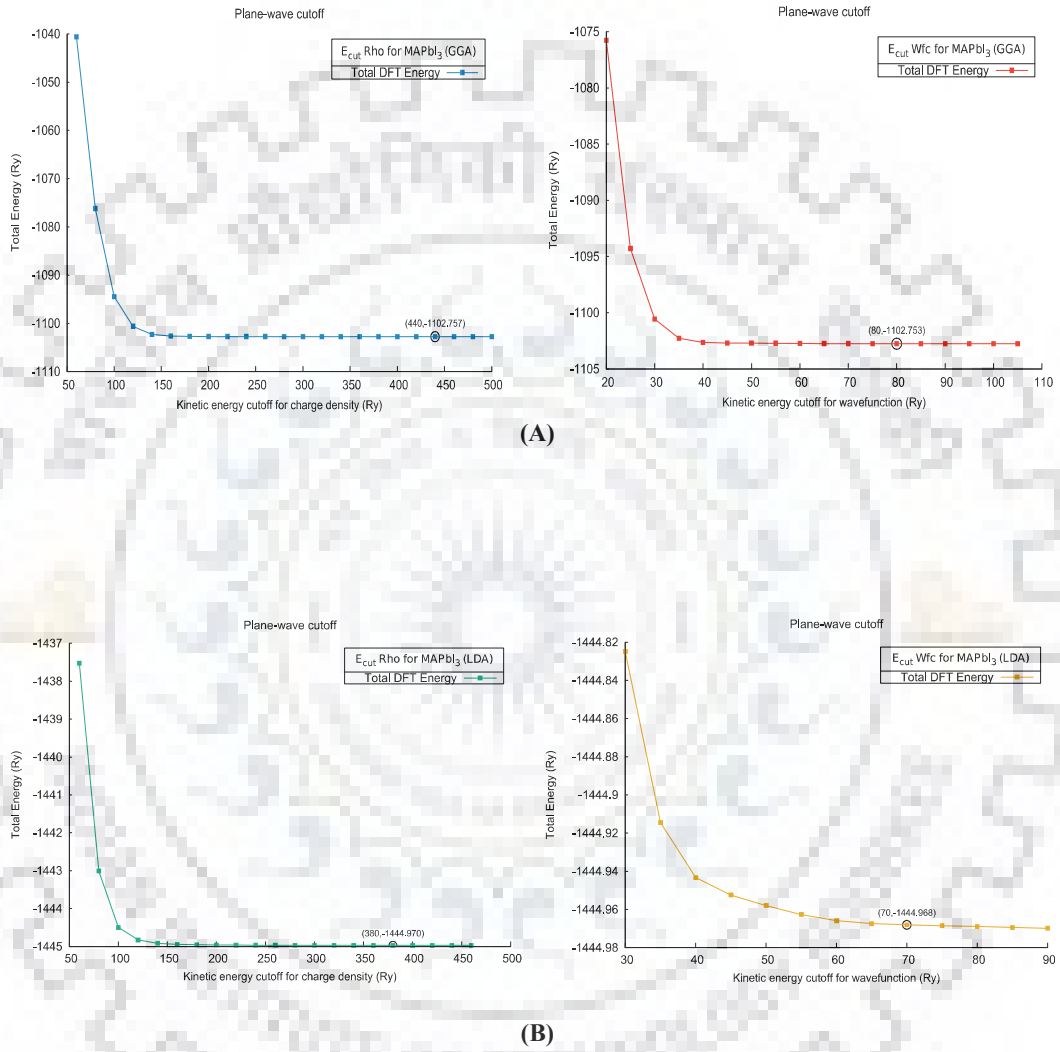

Figure 6.1: Kinetic energy cut-off calculation for $MAPbI_3$ using (A) GGA, (B) LDA approximation.

As it is evident from the above convergence plot of kinetic energy cut-off for electron density and wave-function, the cut-off values for the respective kinetic energy is being successfully achieved. We can see that the kinetic energy cut-off values of LDA approximation is less than cut-off values of GGA, being lesser value of kinetic energy cut-off represents less number of plane waves required for the electronic structure calculation.

Convergence results for Methyl Ammonium Lead Bromide ($MAPbBr_3$):

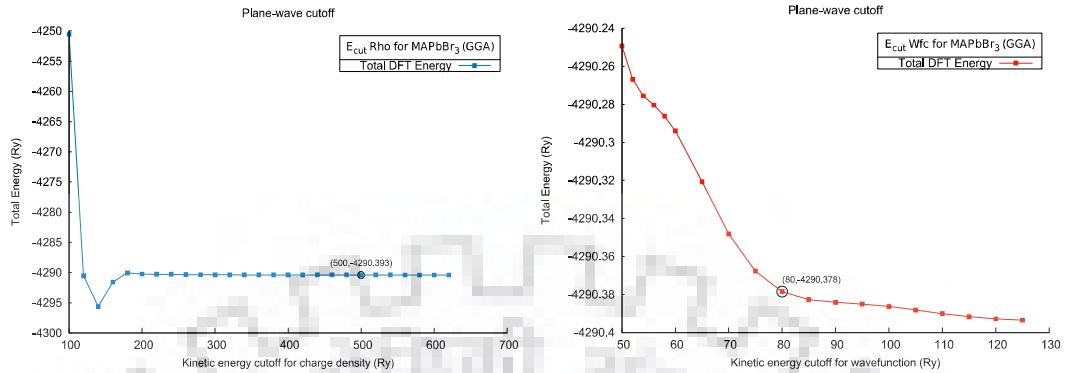

(A)

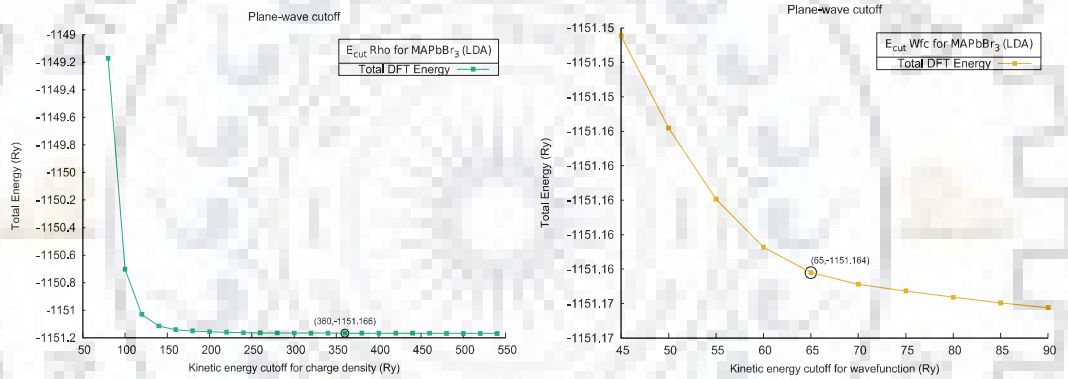

(B)

Figure 6.2: Kinetic energy cut-off calculation for $MAPbBr_3$ using (A) GGA, (B) LDA approximation.

Similarly as in previous convergence plot, this convergence plot for $MAPbBr_3$ also successfully results in good converging cut-off values for kinetic energy (plane-waves). The chosen kinetic energy cut-off are selected randomly after satisfying minimum convergence criteria of 1 x 10^{-3} Ry. All the DFT energy calculation done for the convergence plot includes only gamma point calculation to avoid enormous amount of time for the parameters that can be approximated by this method as well.

Convergence results for Methyl Ammonium Lead Chloride ($MAPbCl_3$):

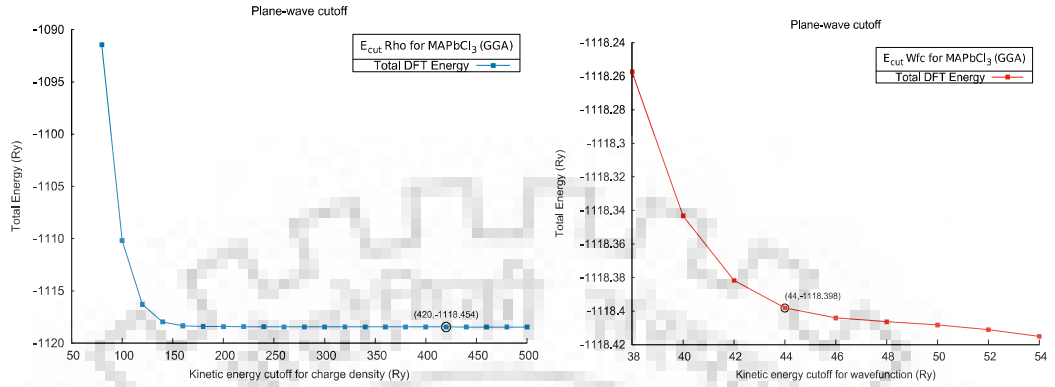

(A)

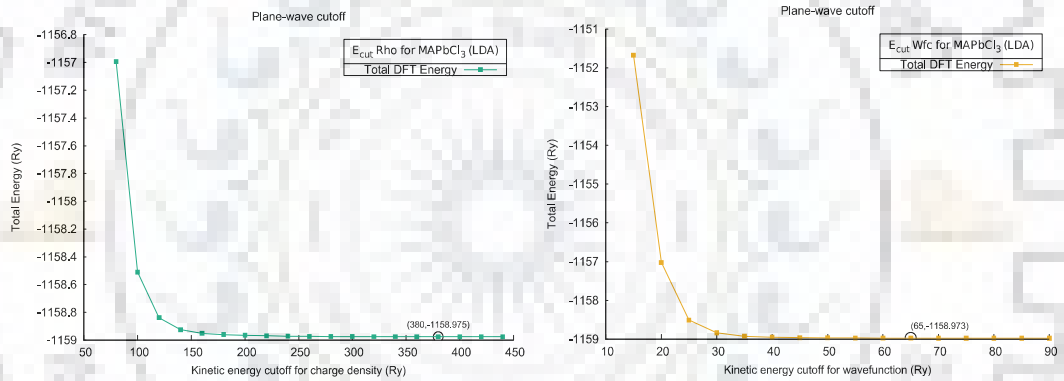

(B)

Figure 6.3: Kinetic energy cut-off calculation for $MAPbCl_3$ using (A) GGA, (B) LDA approximation.

Similar calculation is done for the $MAPbCl_3$ to acquire the kinetic energy cut-off values. The table of kinetic energy cut-off values of electron density (ecut-Rho) and wave-function (ecut-Wfc) calculated for all three perovskite materials using both exchange-correlation approximation, is shown below,

Ecut (Ry)	$MAPbCl_3$		$MAPbBr_3$		$MAPbI_3$	
	LDA	GGA	LDA	GGA	LDA	GGA
Wfc	65	44	65	80	70	80
Rho	380	420	360	500	380	440

Table 6.1: Kinetic energy cut-off values for electron density (ecut-Rho) and wave-function (ecut-Wfc).

Since the plane wave cut-off for electron density (Rho) and wave-function (Wfc) are properties of the pseudopotentials used for the calculation, the absolute value of energy do not represent any physical meaning but energy difference do. The convergence of energy with respect to plane wave cut-off for wave-function is expected due to the variational principle. So firstly, I checked convergence of energy w.r.t. the ecut-Rho having "ecut-Rho=4*ecut-Wfc". With converged ecut-Rho value, calculation of ecut-Wfc is done until the energy convergence vanishes. The energy convergence criteria for this section is set at 1 x 10^{-3} Ry for both ecut-Rho and ecut-Wfc. The plots shown above represents successful estimation of kinetic energy (plane wave) cut-off for electron density and wave-function without compromising the accuracy and calculation complexity. The converged values for cut-off are represented by encircled data-point in the convergence plot using both local density approximation (LDA) and generalised gradient approximation (GGA).

6.2 Optimized Crystal Structures:

Methyl Ammonium Lead Iodide ($MAPbI_3$):

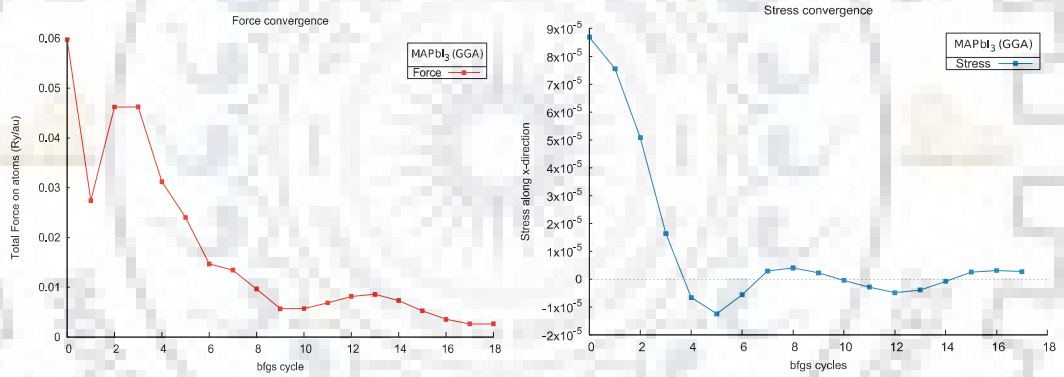

(A)

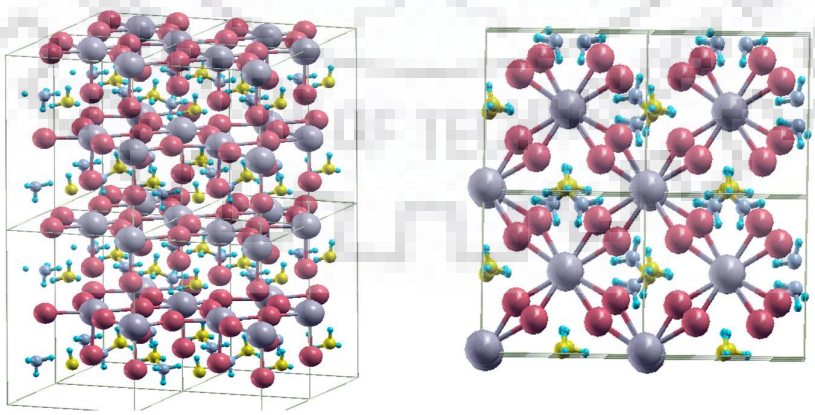

(B)

Figure 6.4: (A) Total force on atoms (left), stress convergence (right), and (B) optimized crystal structure of $MAPbI_3$, orthographic view (left), top view (right).

Methyl Ammonium Lead Bromide ($MAPbBr_3$):

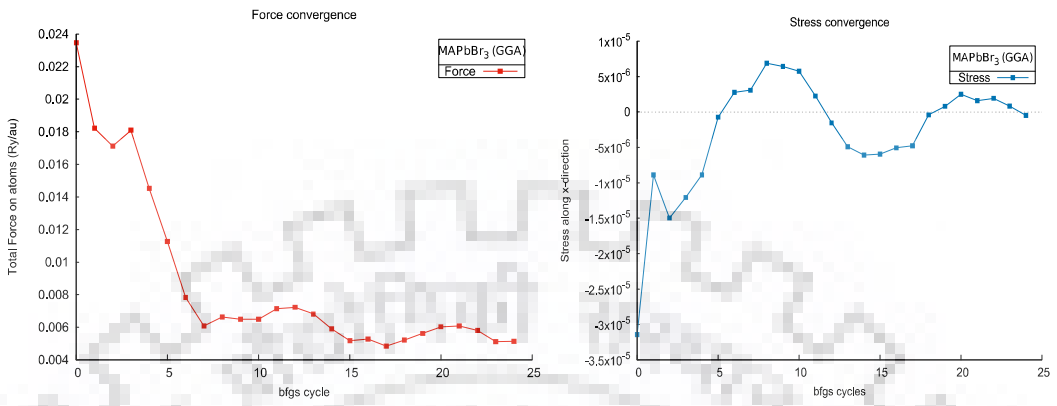

(A)

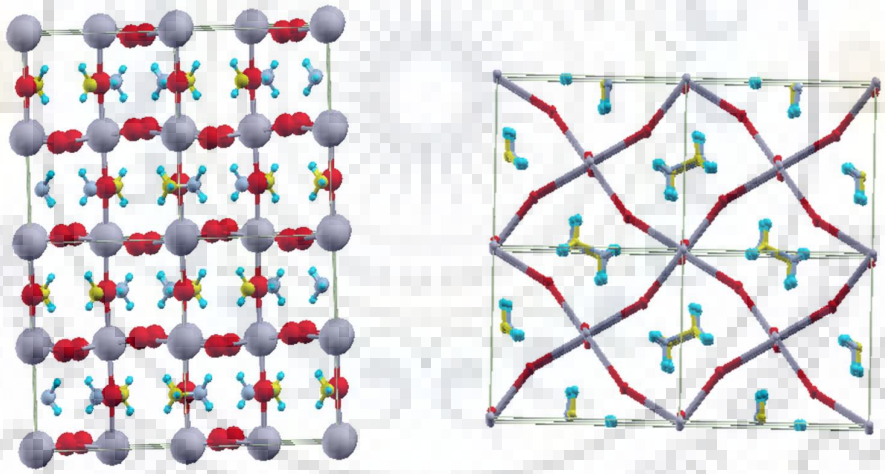

(B)

Figure 6.5: (A) Total force on atoms (left), stress convergence (right), and (B) optimized crystal structure of $MAPbBr_3$, side view (left), stick model top view (right).

Methyl Ammonium Lead Chloride ($MAPbCl_3$):

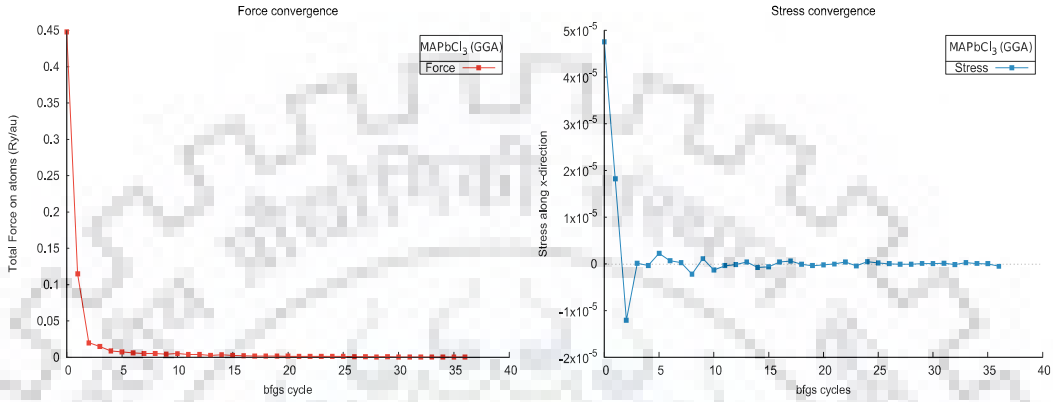

(A)

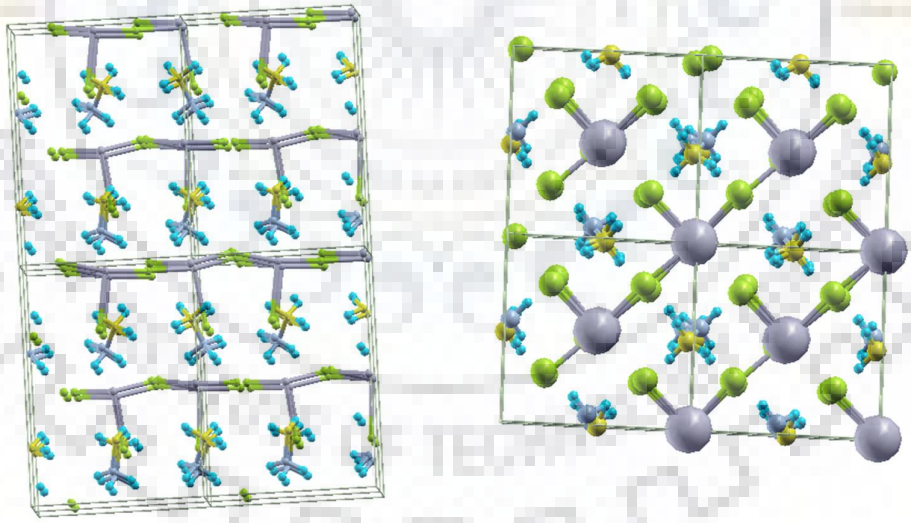

(B)

Figure 6.6: (A) Total force on atoms (left), stress convergence (right), and (B) optimized crystal structure of $MAPbCl_3$, stick model side view (left), top view (right).

All the convergence plots and optimized perovskite crystal structures shown till now, are optimized (calculated) using vc-relax method native to Quantum Espresso DFT package considering only Generalised Gradient Approximation (GGA). Since the GGA approximation is better than LDA approximation so only GGA based optimized structure

and crystal parameters are discussed here. However, the total force and stress covergence for the LDA based optimization is shown as below,

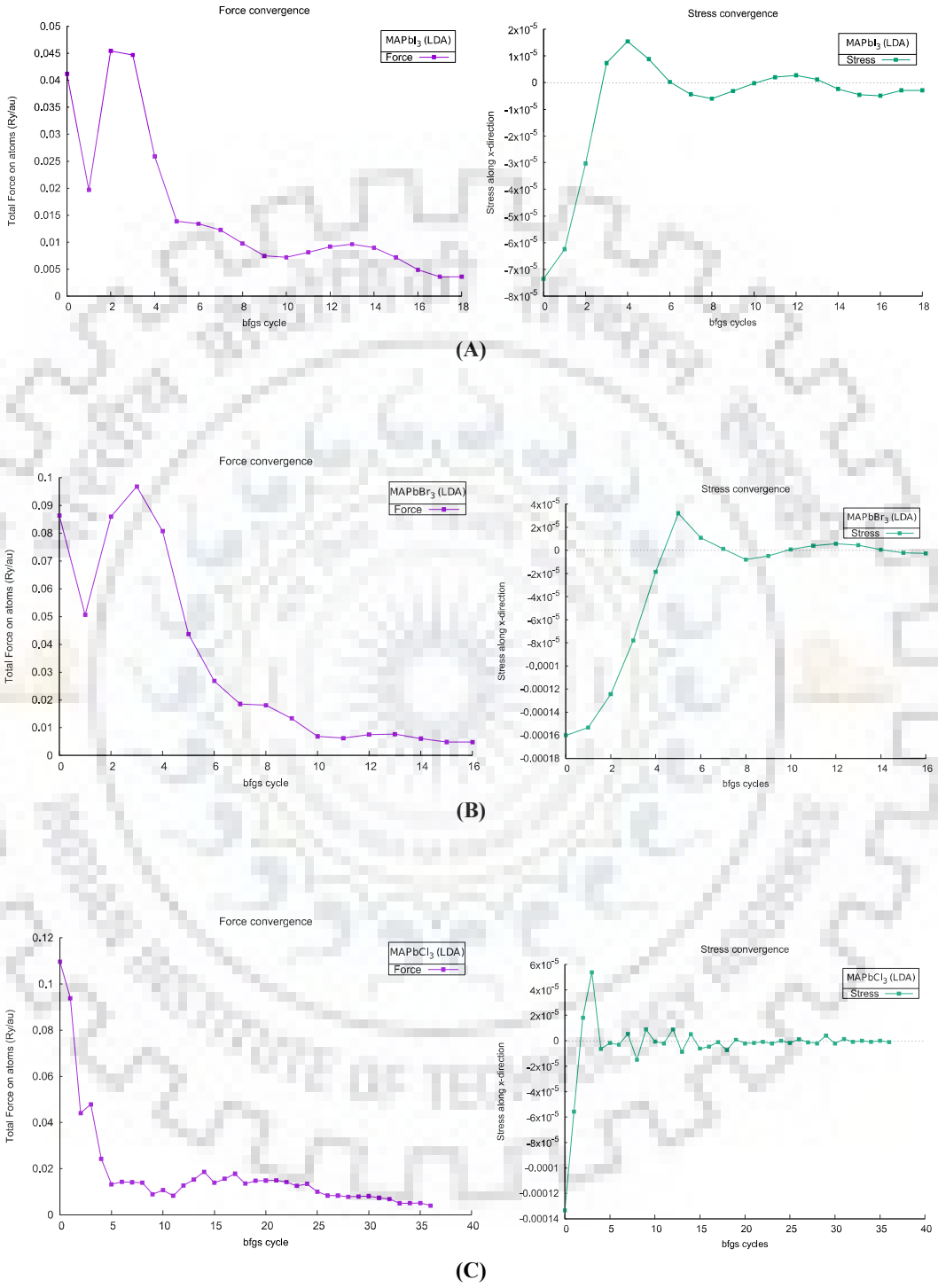

Figure 6.7: Total force (left) and stress (right) convergence with each bfgs iteration for (A) $MAPbI_3$, (B) $MAPbBr_3$, and (C) $MAPbCl_3$ perovskites using LDA approximation.

Optimized structure parameters calculated using generalised gradient approximation (GGA) are represented in the following table,

Material	Optimized Lattice Parameters (Å)			Input Crystal Parameters (Å)		
	a	b	c	a	b	c
$MAPbI_3$	8.9040	8.9195	13.2242	8.6953	8.7153	12.8347
$MAPbBr_3$	7.9789	8.8240	12.1265	8.0208	8.8175	12.3875
$MAPbCl_3$	8.1614	8.2542	11.4896	8.2179	8.3185	12.3499

Table 6.2: Optimized (Calculated) lattice parameters using GGA

Parameters	X=I, Br, Cl		$MAPbI_3$	$MAPbBr_3$	$MAPbCl_3$
Bond Angle(°)	H-C-H		110.462	110.430	110.228
	H-N-H		107.298	107.482	107.305
	X-Pb-X	Equatorial	86-92	83-96	88-89
		Axial	171	180	172-175
Bond Length(Å)	C-H		1.09	1.09	1.09
	N-H		1.04	1.03	1.03
	N-C		1.49	1.49	1.49
	Pb-X		3.24	3.04	2.88

Table 6.3: Optimized perovskite structural parameters using GGA

The crystal structures of perovskites are taken as CIF input from the crystallography open database (COD). The crystal structure taken as input for $MAPbI_3$, $MAPbBr_3$, and $MAPbCl_3$ was tetragonal, orthorhombic and orthorhombic respectively. Since the lifetime of orthorhombic $MAPbI_3$ was very short, I selected tetragonal phase for the computation. The optimization of crystal structures were carried out by the method as described in the computation details section. All the structures transformed into orthorhombic phases after successful crystal structure optimization. In $MAPbX_3$, each Pb (lead) atom is surrounded by six X (halide) atoms, with four X atoms in the equatorial direction and two X atoms in the axial direction. The lattice parameters are represented in the **Table 6.2**. With change in X from I to Br to Cl, lattice constants (b and c) decreases slightly. It is known from the literature that GGA (PBE) functional tends to over-calculate values of lattice constants for semiconductors, ionic solids and metals. Here the lattice parameters calculated from GGA approximation seems to overestimate the parameters available in literature.

6.3 Electronic Structures

6.3.1 Methyl Ammonium Lead Iodide ($MAPbI_3$):

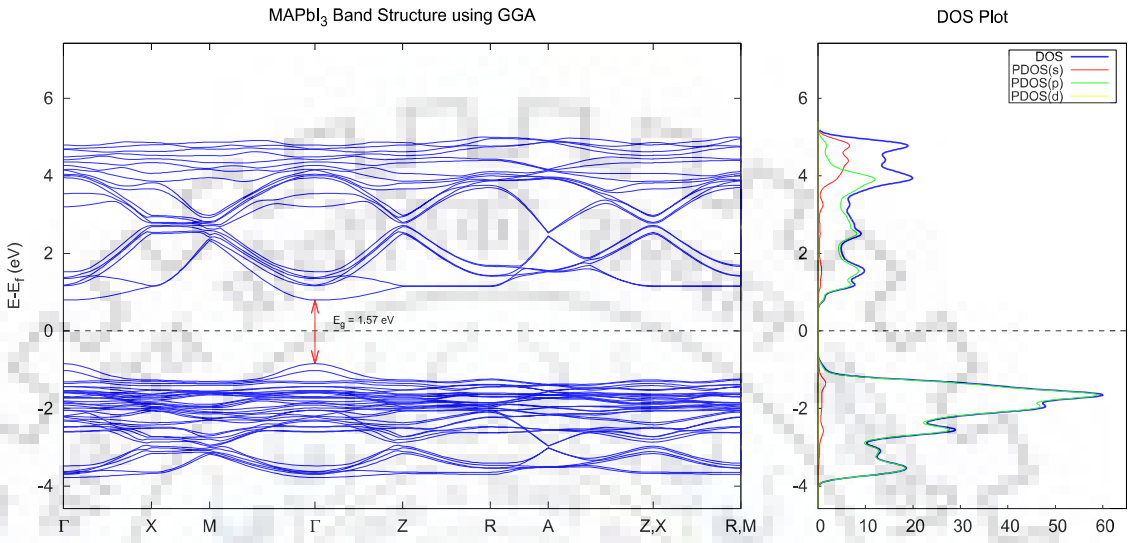

(A)

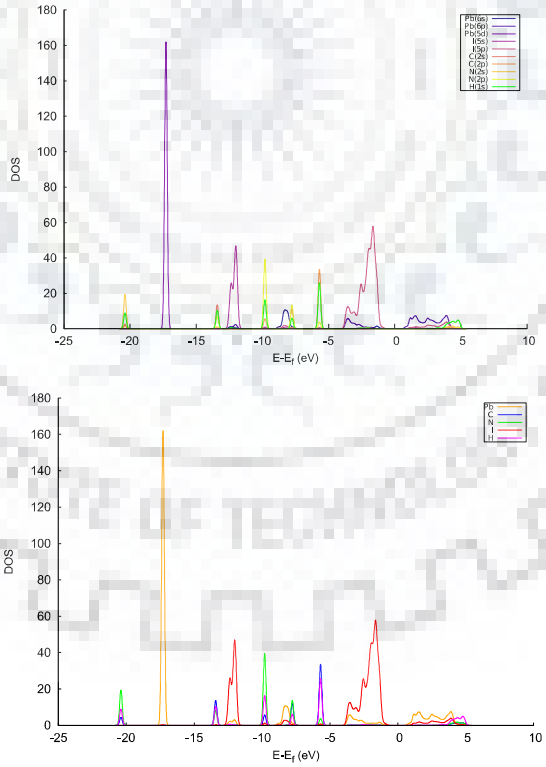

(B)

Figure 6.8: Electronic structure of $MAPbI_3$ using GGA, (A) Band structure + DOS, (B) PDOS orbital-wise (upper), atom-wise (below).

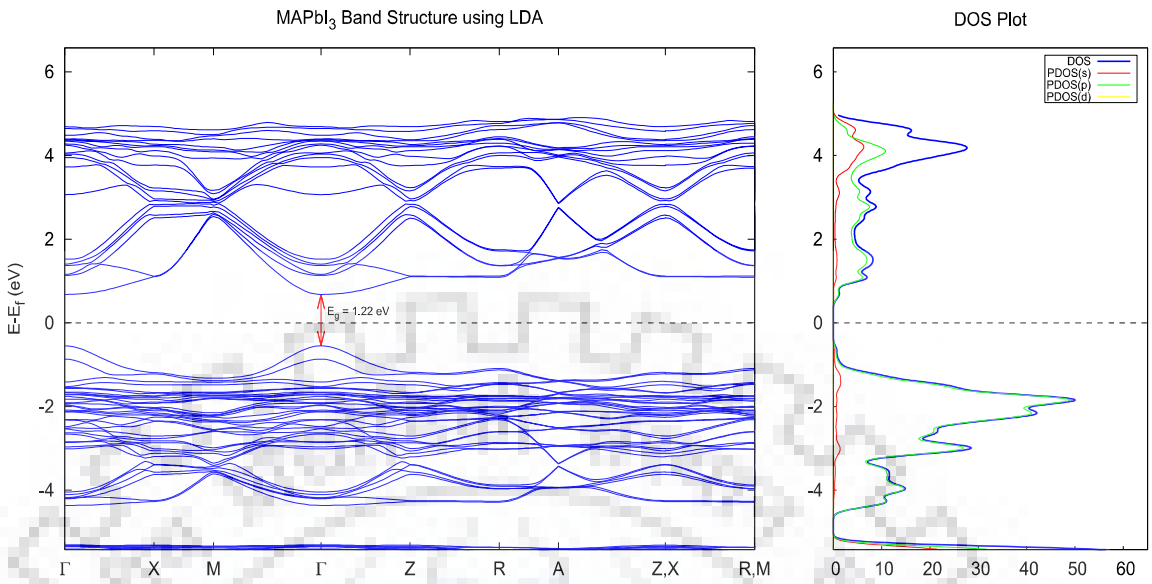

(A)

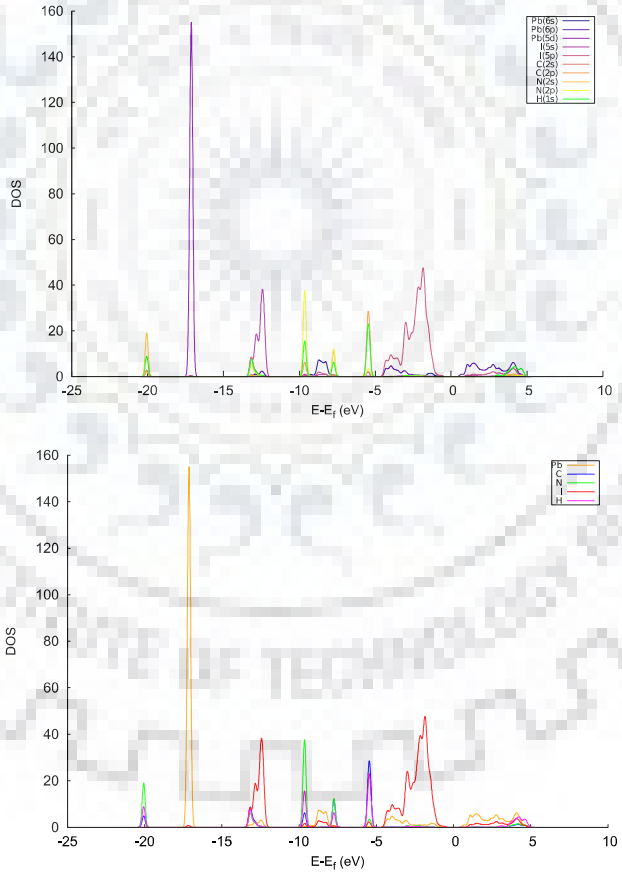

(B)

Figure 6.9: Electronic structure of $MAPbI_3$ using LDA, (A) Band structure + DOS, (B) PDOS orbital-wise (upper), atom-wise (below).

6.3.2 Methyl Ammonium Lead Bromide ($MAPbBr_3$):

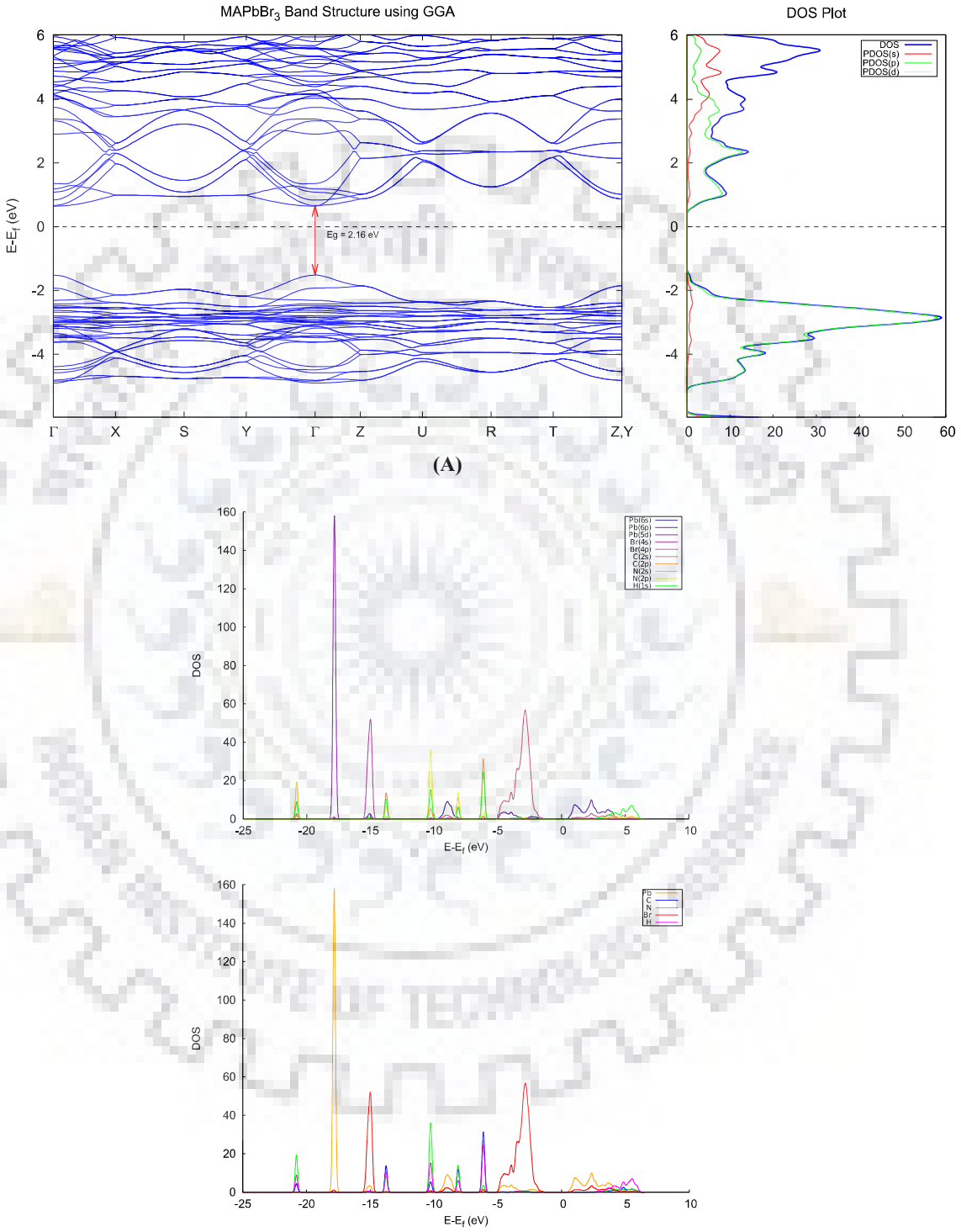

Figure 6.10: Electronic structure of $MAPbBr_3$ using GGA, (A) Band structure + DOS, (B) PDOS orbital-wise (upper), atom-wise (below).

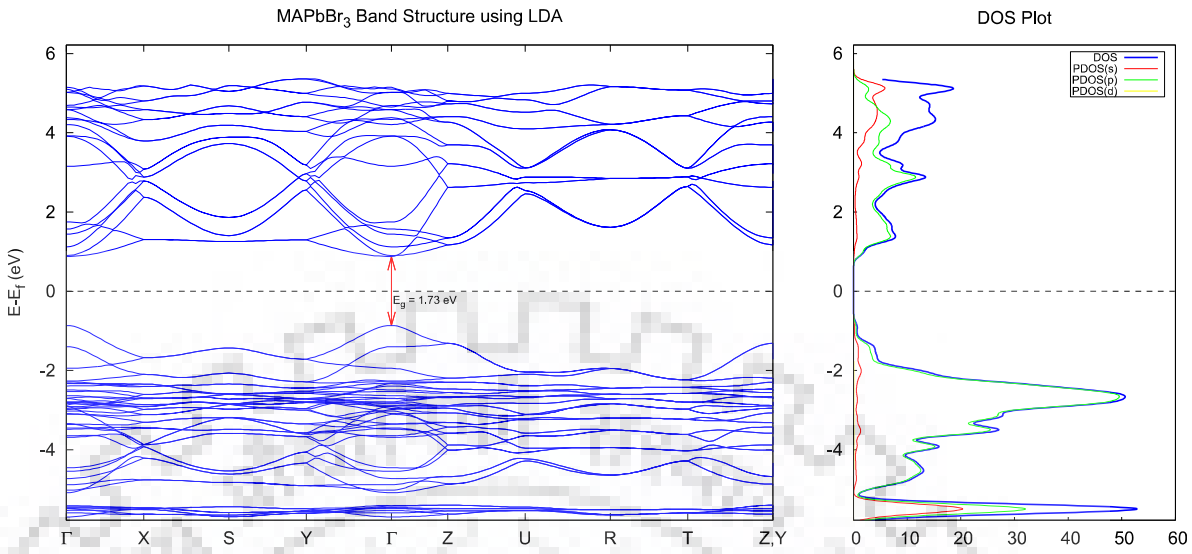

(A)

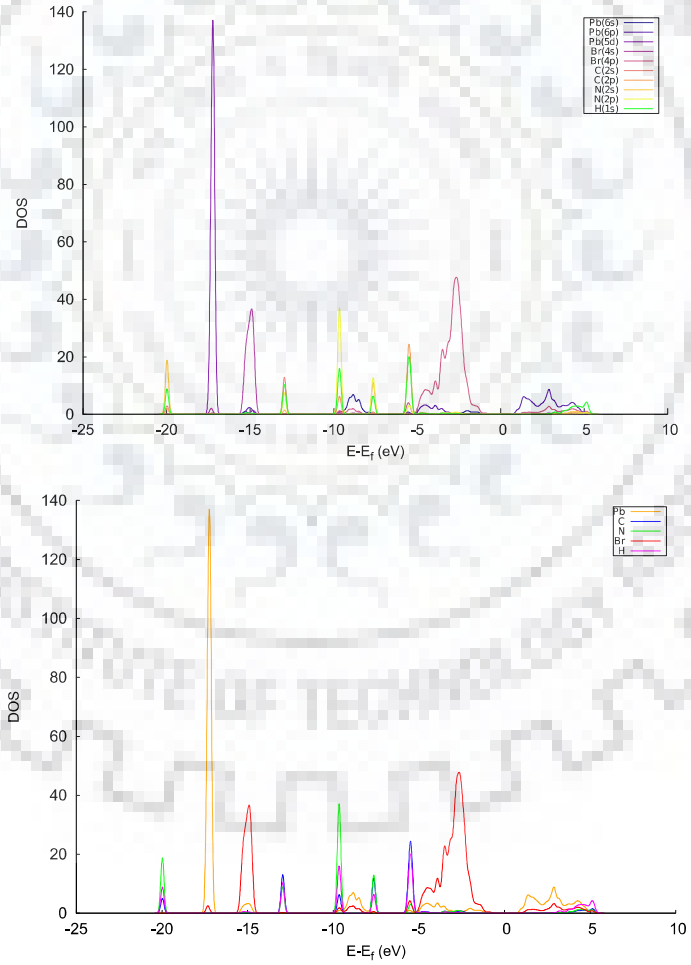

(B)

Figure 6.11: Electronic structure of $MAPbBr_3$ using LDA, (A) Band structure + DOS, (B) PDOS orbital-wise (upper), atom-wise (below).

6.3.3 Methyl Ammonium Lead Chloride ($MAPbCl_3$):

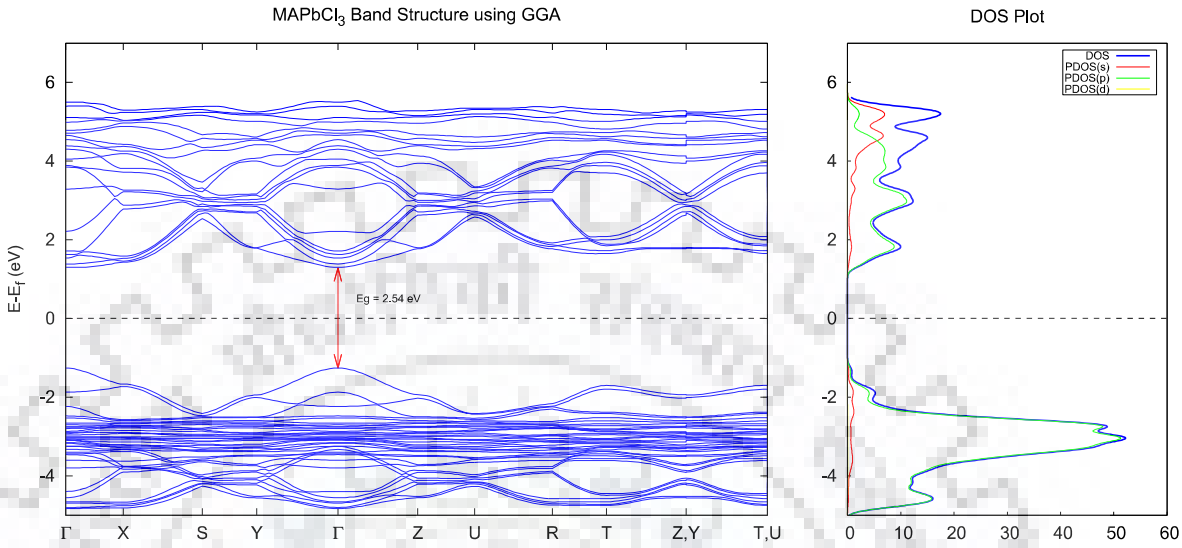

(A)

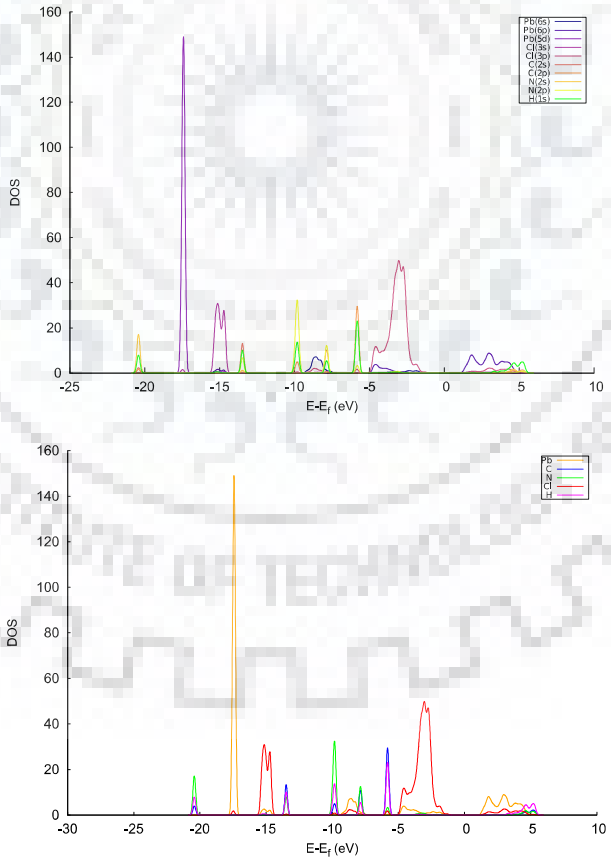

(B)

Figure 6.12: Electronic structure of $MAPbCl_3$ using GGA, (A) Band structure + DOS, (B) PDOS orbital-wise (upper), atom-wise (below).

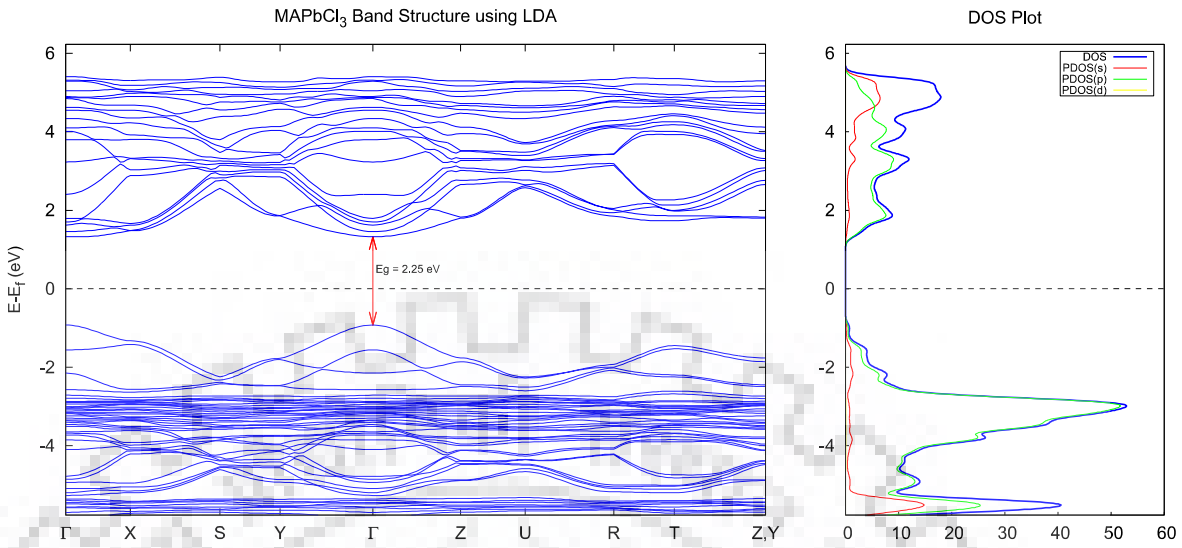

(A)

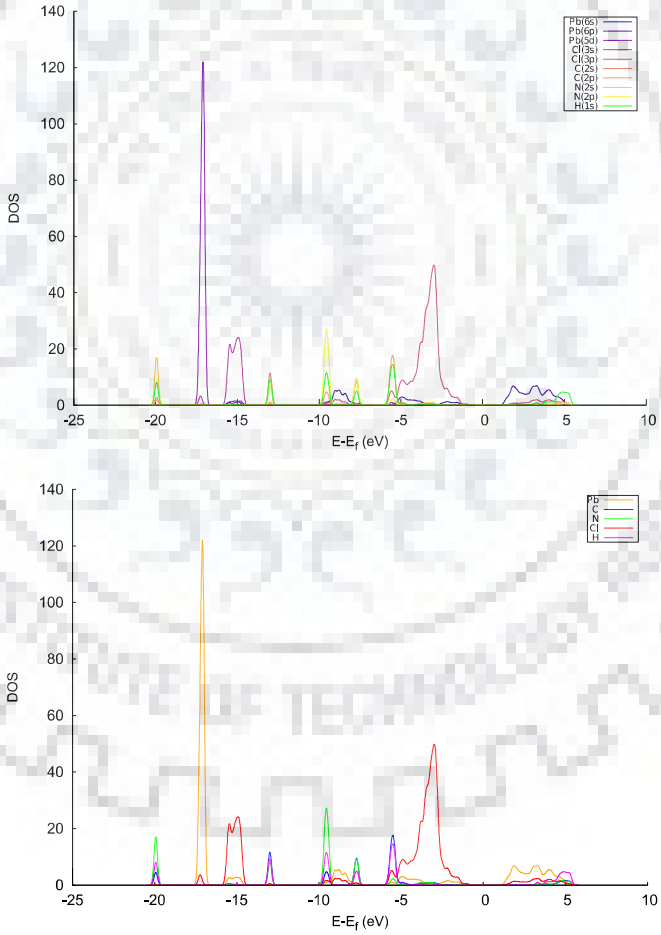

(B)

Figure 6.13: Electronic structure of $MAPbCl_3$ using LDA, (A) Band structure + DOS, (B) PDOS orbital-wise (upper), atom-wise (below).

It is clear from the above energy band diagrams that the energy band-gap achieved is direct band-gap type for all the structures with both exchange-correlation approximations. The energy band-gap is found by calculating the difference between valence band maximum (VBM) and conduction band minimum (CBM) taking the fermi level as reference which is set to be zero. The VBM and CBM are found at the same crystal momentum value (k) i.e. gamma point (Γ) making energy band-gap type to direct band gap. The values of energy band-gap for all the calculations with experimental energy band-gap values and band-gap for gamma only calculation, are represented in the **Table 6.4** below,

Material	$MAPbI_3$		$MAPbBr_3$		$MAPbCl_3$	
	LDA	GGA	LDA	GGA	LDA	GGA
E_{gap}(eV)	1.22	1.57	1.73	2.16	2.25	2.54
$E_{gap(gamma)}$(eV)	1.11	1.43	1.62	2.05	2.14	2.47
$E_{gap-exp}$(eV)	1.58		2.31		2.92	

Table 6.4: Energy band-gap values from DFT calculations and experimental method.

For a better and deep understanding of energy bands and orbital dependence, density of states (DOS) and projected density of states (PDOS) plots are also represented in the previous section. The computational details of it, are represented in computational details section.

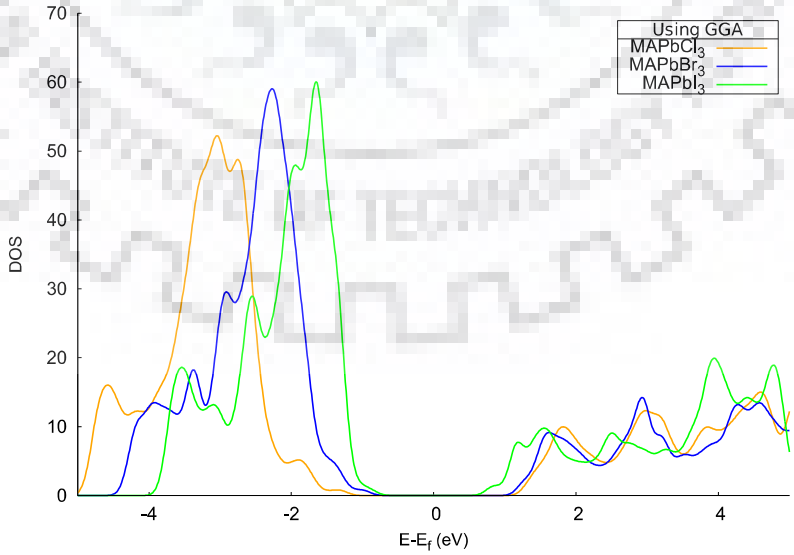

(A)

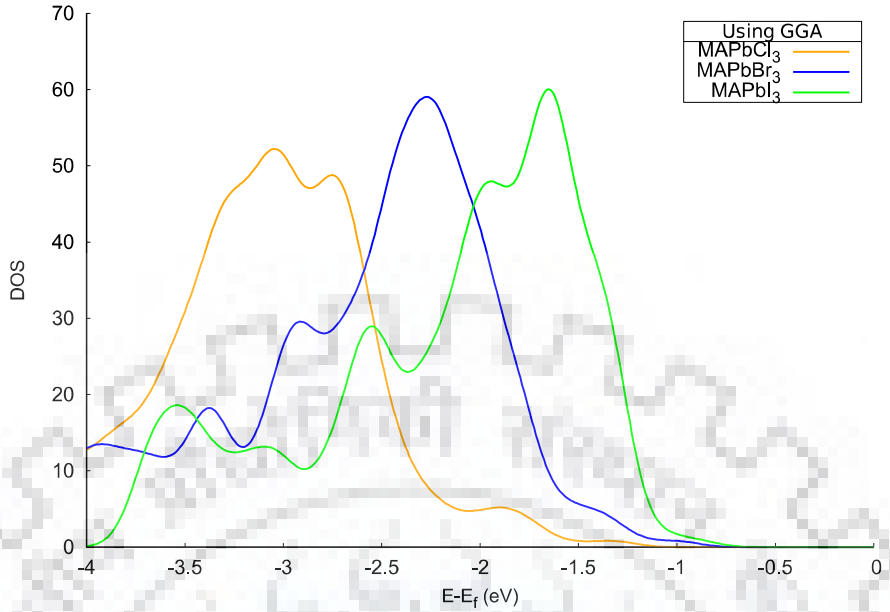

(B)

Figure 6.14: (A) $MAPbX_3$ (X=Cl, Br, I) DOS plot around valence band and conduction band region, (B) The downward shifting of valence band with X=I to Cl.

The calculated band gap values as in **Table 6.4**, are in close agreement with the experimental band gap values. The band structure and the density of states plot, possess almost similar configuration and electronic properties. All the band gap values for the systems are acquired at the gamma point (Γ). The energy band gap value of all three perovskites are in great agreement of band gap values reported in literature as well. The energy band gap value increases with halide X = I to Br to Cl which follows the same pattern as of experimental band gap values.

On examining the density of states diagram **Figure 6.14** and PDOS plots for all the computations, we see that the valence band (VB) for each material calculation is mainly contributed by the p state of the X (I, Br, Cl) atoms and moderately dominated by the s state of the lead (Pb) atoms. In other hand, the conduction band (CB) is mainly dominated by the p state of the lead (Pb) atoms. From the research submitted by Yin et al., they studied constitution of valence and conduction band and find out that there is coupling between the s state of Pb and p state of halide (X), played a key role in band structure and other aspects like effective mass. Since the VBM and CBM is dominated by only X (I, Br, Cl) and Pb atoms, it is evident that the band gap is largely dependent on the X-Pb (I, Br, Cl) bond. It is evident from the above figure that valence band shift downwards with X = I to Br to Cl. With change in X from I to Br to Cl, the bond length decreases due to high electronegativity of Cl. This decrease in the Pb-X bond length leads to the more orbital overlapping between Pb and X. This increased interaction between the Pb and X atoms can be the reason for the increase in the band gap value for X (I to Br to Cl).

6.4 Bulk Modulus

Methyl Ammonium Lead Iodide ($MAPbI_3$)

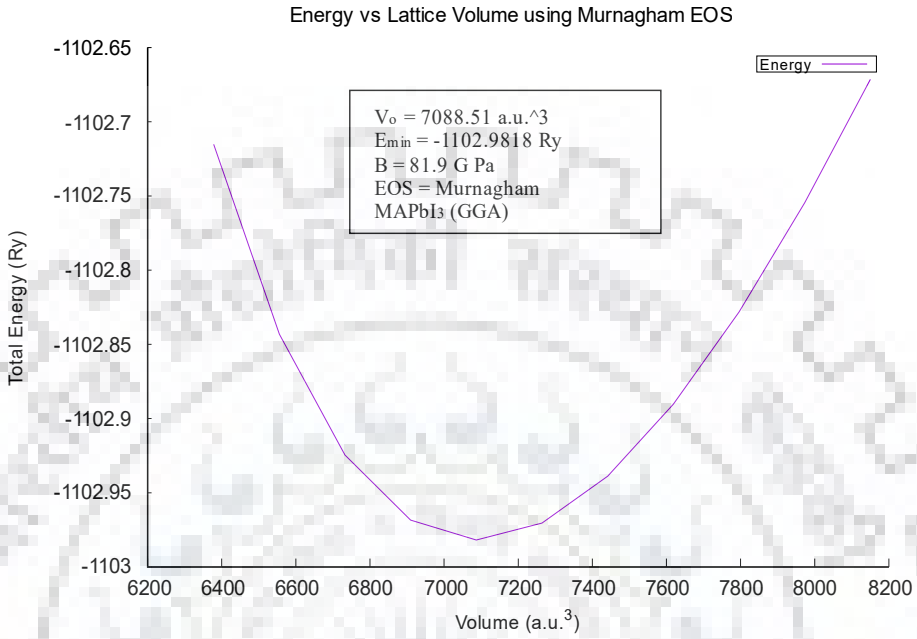

Figure 6.15: E-V curve of $MAPbI_3$ using GGA with Murnagham equation of state (EOS) fit.

Methyl Ammonium Lead Bromide ($MAPbBr_3$)

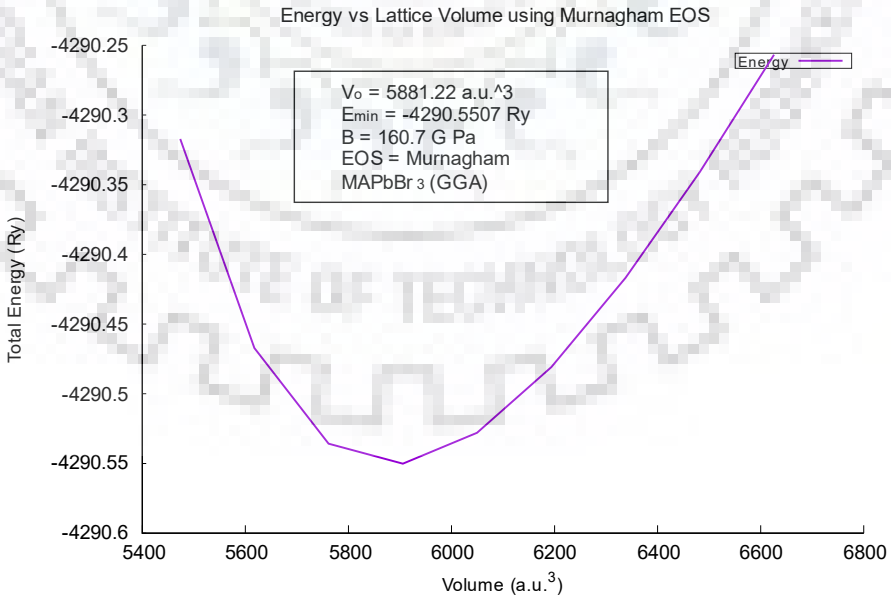

Figure 6.16: E-V curve of $MAPbBr_3$ using GGA with Murnagham equation of state (EOS) fit.

Methyl Ammonium Lead Chloride ($MAPbCl_3$)

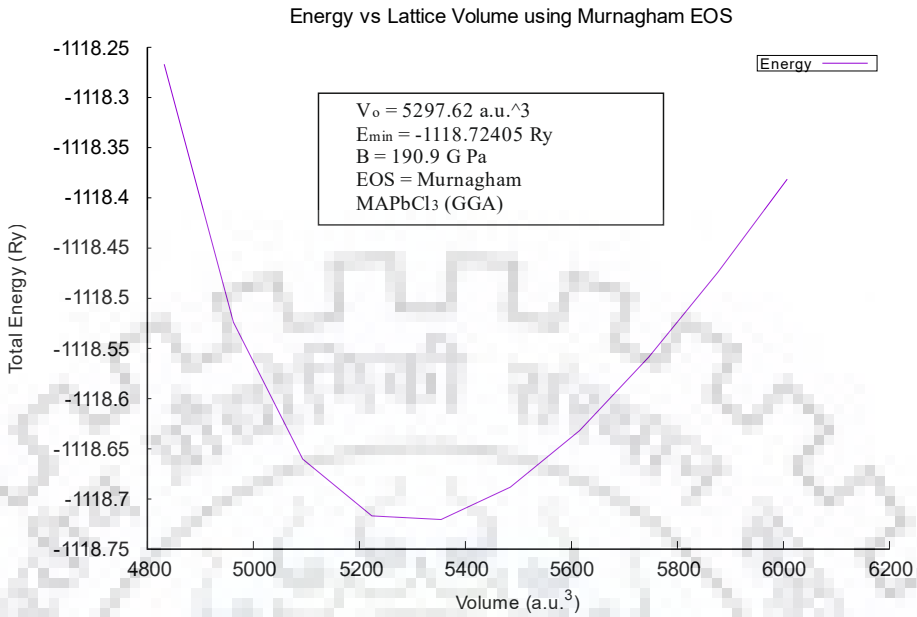

Figure 6.17: E-V curve of $MAPbCl_3$ using GGA with Murnagham equation of state (EOS) fit.

The theory and calculation done for the bulk modulus calculation is already shown in the computational chapter. The remaining bulk modulus values of perovskite systems are represented in the following **Table 6.5**,

Equation of state	$MAPbI_3$ (in G Pa)		$MAPbBr_3$ (in G Pa)		$MAPbCl_3$ (in G Pa)	
	LDA	GGA	LDA	GGA	LDA	GGA
Birch (1st order)	107.5	83.4	260.5	198.3	303.2	224.4
Birch (2nd order)	106.4	82.6	382.7	266.4	311.3	216.6
Keane	103.8	81.9	193.3	139.2	259.2	188.8
Murnagham	105.3	81.9	208.6	160.7	257.3	190.9

Table 6.5: Bulk Modulus (B) of $MAPbX_3$ perovskites using LDA and GGA approximation by fitting with 4 equation of states.

Among all the equation of states, Murnagham equation of states represents close bulk modulus values to the reported data. LDA overestimated the bulk modulus values more than GGA. For the calculation of bulk modulus, the direction of force applied is along the largest dimension of respective crystal lattice.

CHAPTER – 7

CONCLUSION & FUTURE ASPECTS

7 Conclusion & Future Aspects

In summary, first principle DFT calculations have been performed to examine structural and electronic properties of the $MAPbX_3$ (X = I, Br, Cl) materials using the local density functional and generalised gradient functional. This study demonstrates that the local density functional largely underestimates the energy band gap values in comparison to the generalized gradient functional. Similar trends of LDA underestimation is observed in electronic properties and structure optimization. The optimized crystal lattice parameters are 8.90, 8.91, 13.22 Å; 7.98, 8.82, 12.13 Å and 8.16, 8.25, 11.49 Å for $MAPbX_3$ (X = I, Br, Cl) using GGA functional. The Methyl Ammonium part of the structure remains same for all three perovskites. In general, it is clear from the energy band diagrams that the energy bands are very similar for $MAPbX_3$ (X = I, Br, Cl) exhibiting direct band gap at gamma (Γ) point of the Brillouin zone. Since VBM in each perovskite is dominated by the p-orbital of the halide (X= I, Br, Cl) and partly s-orbital of the Pb atoms. Whereas the CBM is contributed by the p-orbital of the Pb atom. These features suggests possible coupling between lone pair s-orbital of Pb atom and p-orbital of halogen (X) atoms at VBM which is an anti-bonding site. This coupling between p-X and s-Pb can play an important role in electronic structure. With X= I to Br to Cl, the bond length of Pb-X decreases and it results in increased overlapping (interaction) between the Pb and X atoms. This increased interaction can be responsible for the increased band gap. From the optimized structure, it can be seen that the Methyl Amine (MA^+) parameters like C-H, N-H, and C-N bond length remained same with all three perovskite structure, so it cannot have direct impact on the band gap value. Also there is no MA related atoms contribution in the band edge. But it is possible that MA can have indirect impact on the band structure with some weak interaction by affecting Pb-X bond.

The bulk modulus (B) is also in agreement with the literature data for the Murnagham based equation of state fit. The local density functional seems to overestimate the bulk modulus using every equation of state fit. The possible reason for this behaviour cannot be deduced from this observation. The bulk modulus values for the generalised gradient functional is 81.9, 160.7, and 190.9 G Pa for $MAPbX_3$ (X= I, Br, Cl) using Murnagham equation of state E-V curve fitting. The force applied for the calculation is along the largest crystal dimension so that the perturbation is not too abrupt to give the E-V curve a parabolic fitting.

Any theoretical calculation has an advantage over the experimental method as it does not require any special conditions in the laboratory for experiment to work. Almost all theoretical calculations are less time consuming and produces significantly less error. The first principle DFT is one such theoretical quantum mechanical modelling method. With development in quantum mechanical theories, DFT is now less time consuming and produces very accurate results. The first principle DFT calculation of perovskite provides the constituent element-wise contribution in the electronic structure and thus making possible band gap engineering by changing the constituent elements composition in the input crystal lattice. Similarly other properties can also be regulated according to our

needs. Also one can model any hypothetical (extremely unstable) material and try to extract the properties out of it using first principle DFT.

REFERENCES

1. P. Hohenberg, W. Kohn, “Inhomogeneous electron gas,” *Phys. Rev.* 136, B864. doi.org/10.1103/PhysRev.136.B864, Vol. 136, Iss. 3B, November 1964.
2. M. A. Pena, J. L. G. Fierro, “Chemical Structures and Performance of Perovskite oxides,” *Chemical Reviews*, vol. 101, pp. 1981-2018, 2001.
3. W. Cao, J. Xue, “Recent progress in organic photovoltaics: device architecture and optical design,” *Energy Environ Sci*, 7 (7) (2014), pp. 2123-2144.
4. J. Cui, H. Yuan, J. Li, X. Xu, Y. Shen, H. Lin, “Recent progress in efficient hybrid lead halide perovskite solar cells,” *Sci Technol Adv Mater* (2016).
5. S. Kazim, M. K. Nazeeruddin, M. Grtzel, S. Ahmad, “Perovskite as light harvester: a game changer in photovoltaics,” Angew Chem Int Ed, 53 (11) (2014), pp. 2812-2824.
6. X. Tong, F. Lin, J. Wu, Z.M. Wang, “High performance perovskite solar cells,” *Adv Sci* (2015).
7. H.S. Jung, N.G. Park, “Perovskite solar cells from materials to devices,” *Small*, 11 (1) (2015), pp. 10-25.
8. N.-G. Park, “Organometal perovskite light absorbers toward a 20 % efficiency low-cost solid-state mesoscopic solar cell,” *J Phys Chem Lett*, 4 (15) (2013), pp. 2423-2429.
9. A.K. Chilvery, A.K. Batra, B. Yang, K. Xiao, P. Guggilla, M.D. Aggarwal, “Perovskites transforming photovoltaics, a mini-review,” *Journal of Photon Energy*, 5 (1) (2015).
10. K. Mahmood, B.S. Swain, A.R. Kirmani, A. Amassian, “Highly efficient perovskite solar cells based on a nanostructured WO 3-TiO 2 core-shell electron transporting material,” *Journal of Material Chemistry A*, 3 (17) (2015), pp. 9051-9057.
11. P. Docampo, F.C. Hanusch, N. Giesbrecht, P. Angloher, A. Ivanova, T. Bein, “Influence of the orientation of methyl ammonium lead iodide perovskite crystals on solar cell performance,” *APL Material*, 2 (8) (2014), p. 081508.
12. N. Ahn, D.-Y. Son, I.-H. Jang, S.M. Kang, M. Choi, N.-G. Park, “Highly reproducible perovskite solar cells with average efficiency of 18.3% and best efficiency of 19.7% fabricated via Lewis base adduct of lead (II) iodide,” *Journal of the American Chemical Society*, 137 (27) (2015), pp. 8696-8699.
13. M.A. Green, A. Ho-Baillie, “Perovskite solar cells: the birth of a new era in photovoltaics,” *ACS Energy Letters*, 2 (2017), pp. 822-830.
14. J.-H. Im, C.-R. Lee, J.-W. Lee, S.-W. Park, N.-G. Park, “6.5% efficient perovskite quantum-dot-sensitized solar cell,” *Nanoscale*, 3 (10) (2011), pp. 4088-4093.
15. J.H. Noh, S.H. Im, J.H. Heo, T.N. Mandal, S.I. Seok, “Chemical management for colorful, efficient, and stable inorganic-organic hybrid nanostructured solar cells,” *Nano Letters*, 13 (4) (2013), pp. 1764-1769.
16. Thomas, L. H. (1927), "The calculation of atomic fields," *Proceedings of Cambridge Philosophical Society* 23(5):542–548.
17. Fermi, Enrico (1927), "A Statistical Method for Determining Some Atom Properties,” *Rend. Accad. Naz. Lincei.* 6: 602–607.

18. Dirac, P. A. M. (1930), "Note on exchange phenomena in the Thomas-Fermi atom," *Proc. Camb. Phil. Soc.* 26 (3): 376–385.
19. Hartree, D. R. (1928), "The Wave Mechanics of an Atom with a Non-Coulomb Central Field," *Mathematical Proceedings of Cambridge Philosophical Society* 24 (1): 89.
20. Fock, VZ Physik (1930), "Approximation method for solving the quantum mechanical multibody problem" 61: 126.
21. Slater, J. C. (1928), "The Self Consistent Field and the Structure of Atoms," *Phys. Rev.* 32 (3): 339.
22. P. Hohenberg, W. Kohn (1964), "Inhomogeneous electron gas," *Phys. Rev.* 136, B864, Vol. 136, Iss. 3B.
23. Kohn, Walter; Sham, Lu Jeu (1965), "Self-Consistent Equations Including Exchange and Correlation Effects," *Physical Review*, 140 (4A): A1133–A1138.
24. Y. H. Chang, C. H. Park, K. Matsuishi, "First-principles study of the structural and the electronic properties of the lead-halide-based inorganic-organic perovskites $CH_3NH_3PbX_3$ and $CsPbX_3$ (X=Cl, Br, I)," *J. Korean Phys. Soc.*, 2004, 44, 889–893.
25. I. Borriello, G. Cantele, D. Ninno, "Ab initio investigation of hybrid organic-inorganic perovskites based on tin halides," *Phys. Rev. B: Condensed Matter Mater. Phys.*, 2008, 77, 235214.
26. Y. Wang, T. Gould, J. F. Dobson, H. M. Zhang, H. G. Yang, X. D. Yao and H. J. Zhao, "Recent progress in organic–inorganic halide perovskite solar cells: mechanisms and material design," *Phys. Chem. Chem. Phys.*, 2014, 16, 1424-1429.
27. J. C. Menendez-Proupin, E. Palacios, P. Wahnon and P. Conesa, *Phys. Rev. B: Condensed Matter Mater. Phys.*, 2014, 90, 045207.
28. R. Gottesman, E. Haltzi, L. Gouda, S. Tirosh, Y. Bouhadana and A. Zaban, J. *Phys. Chem. Lett.*, 2014, 5, 2662–2669.
29. G. Murtaza, I. Ahmad, M. Maqbool, H. A. R. Aliabad and A. Afaq, *Chin. Phys. Lett.*, 2011, 28, 117803.
30. G. Murtaza and I. Ahmad, *Physica B*, 2011, 406, 3222–3229.
31. X. Zhu, H. Su, R. A. Marcus, M. E. Michel-Beyerle, *J. Phys. Chem. Lett.*, 2014, 5, 3061.
32. F. Brivio, A. B. Walker, A. Walsh, *APL Materials*, 2014, 2, 081506.
33. T. Minemoto, M. Murata, *Journal of Applied Physics*, 2014, 116, 054505.
34. J. S. Haruyama, K. Sodeyama, L. Han, Y. Tateyama, *J. Phys. Chem. Lett.*, 2014, 5, 2903-2909.
35. K. T. B. Jarvist, M. Frost, F. Brivio, C. H. Hendon, M. van Schilfgaarde, A. Walsh, *Nano Letters*, 2014, 14, 2584.
36. Wei Geng, Le Zhang, Yan-Ning Zhang, Woon-Ming Lau, Li-Min Liu, "First-Principles Study of Lead Iodide Perovskite Tetragonal and Orthorhombic Phases for Photovoltaics," *J. Phys. Chem. C*, 2014, 118 (34), pp 19565–19571.

37. Li Lang, Ji-Hui, Yang, Heng-Rui, Liu, H.J. Xiang, X.G. Gong, "First-principles study on the electronic and optical properties of cubic ABX_3 halide perovskites," *Physics Letters A,* Volume 378, Issue 3, 10 January 2014, 290-293.
38. Edoardo Mosconi, A.B. Paolo Umari, Filippo De Angelis, "Electronic and optical properties of $MAPbX_3$ perovskites (X = I, Br, Cl): a unified DFT and GW theoretical analysis," *Physical Chemistry Chemical Physics*, 2016, 18, 27158-27164.
39. Max Born, J. Robert Oppenheimer (1927), "On the Quantum Theory of Molecules," *Annalen der Physik*. 389 (20): 457–484.
40. Feynman, R. P. (1939), "Forces in Molecules," *Physical Review*, 56 (4): 340.
41. S. M. Blinder (1965), "Basic Concepts of Self-Consistent-Field Theory", *American Journal of Physics,* 33, 431.
42. N. H. March (1983), "Origins-The Thomas–Fermi Theory," S. Lundqvist and N. H. March (eds.), "Theory of the Inhomogeneous Electron Gas," *Plenum Press*. ISBN 978-0-306-41207-3
43. Dirac, Paul A. M. (1926), "On the Theory of Quantum Mechanics," *Proceedings of the Royal Society A.* 112 (762): 661–77.
44. International Centre for Theoretical Sciences, "An Introduction to Density Functional Theory by MK Herbola," Feb14, 2014. https://www.youtube.com/watch?v=g5wI--2GMTU&t=4473s
45. C. Fiolhais, F. Nogueira, M. Marques, "A primer in DFT," Chapter 1 page no. 13, ISBN 3-540-03082-2, Springer-Verlag Berlin Heidelberg New York.
46. J. P. Perdew, A. Zunger (1981), "Self-interaction correction to density-functional approximations for many-electron systems," *Phys. Rev. B.* 23 (10): 5048-5079
47. Matthias Ernzerhof, Gustavo E. Scuseria (1999), "Assessment of the Perdew-Burke-Ernzerhof exchange-correlation functional," *J. Chem. Phys.* 110, 5029.
48. A.D. Becke (1993), "A new mixing of Hartree-Fock and local density-functional theories," *J. Chem. Phys.* 98 (2): 1372-1377.
49. Grabowski, Paul, Burke, Kieron (2014), "Quantum critical benchmark for density functional theory," retrieved from https://www.researchgate.net/publication/237152659_Nonempirical_derivation_of_the_parameter_in_the_B88_exchange_functional
50. Sarah A. Tolba, Kareem M. Gameel, Basant A. Ali, Hossam A. Almossalami, Nageh K. Allam, "The DFT+U: Approaches, Accuracy, and Applications," Book Published: May 16th 2018, DOI: 10.5772/intechopen.72020.
51. Yucheng Liu, Zhoi Yang, Dong Cui, "Two inch sized perovskite $CH_3NH_3PbX_3$ (X=Cl, Br, I) crystals," *Advanced materials*, 27: 5176-5183. doi:10.1002/adma.201502597.